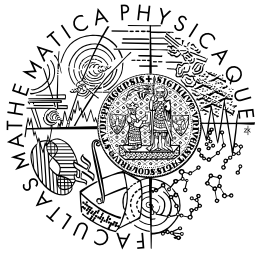

FACULTY
OF MATHEMATICS
AND PHYSICS
Charles University

MASTER THESIS

Hedvika Gedeonová

Study of Time Evolution of Metastable States in Quantum Mechanics

Institute of Theoretical Physics

Supervisor of the master thesis:	RNDr. Přemysl Kolorenč, Ph.D.
Study programme:	Physics
Study branch:	Theoretical Physics

Prague 2019

I declare that I carried out this master thesis independently, and only with the cited sources, literature and other professional sources.

I understand that my work relates to the rights and obligations under the Act No. 121/2000 Sb., the Copyright Act, as amended, in particular the fact that the Charles University has the right to conclude a license agreement on the use of this work as a school work pursuant to Section 60 subsection 1 of the Copyright Act.

In Prague 19.7. 2019 signature of the author

I would like to thank my supervisor Přemysl Kolorenč for his outstanding patience and valuable advice.
My gratitude also belongs to my whole family for their unconditional support and to Kozlíček for all the cups of tea he made for me.

Title: Study of Time Evolution of Metastable States in Quantum Mechanics

Author: Hedvika Gedeonová

Institute: Institute of Theoretical Physics

Supervisor: RNDr. Přemysl Kolorenč, Ph.D., Institute of Theoretical Physics

Abstract: In this thesis, the metastable states are studied. The work focuses on a theoretical model of one or two metastable states decaying into a continuum of states which is bounded from below. We examine the time evolution of such systems and how it is affected by the energy of the metastable state(s) and by the position of the poles of the scattering matrix in the complex plane. We also look closely at the spectral line shape. Numerical integration of a system of differential equations is used for solving the problem of the time evolution and spectral line shape while Freshbach-Fano projection operator formalism is used for finding the position of the poles. The results are compared with first order perturbation theory and with semi-analytical formula obtained from adiabatic elimination of the continuum. The last part of the thesis is dedicated to an application of the model on neon–helium–neon cluster.

Keywords: resonance scattering, decay process, poles of S-matrix, ICD

Contents

Introduction **2**

1 Brief Review of Scattering Theory **3**
1.1 Resonances 4
1.2 Freshbach-Fano Projection Operator Formalism 4
1.3 Decay Processes 7
1.3.1 Fano Model 8
1.3.2 Generalized Fano Model 8
1.3.3 Deviations from Exponential Decay 8
1.3.4 Spectral Line Shape 9

2 The Model **10**
2.1 Isolated Resonance 11
2.2 Two Resonances 11
2.2.1 Adiabatic Elimination of the Continuum 12

3 Results and Discussion **15**
3.1 One Resonance 15
3.2 Two Overlapping Resonances 17

4 Application **40**

Conclusion **50**

Bibliography **51**

Introduction

It has become important over time that the decay processes could be well described and well understood. Since the processes in nature are often too complicated, we have to restrict ourselves to a simple models and their solutions. This thesis offers purely theoretical description of such a simple model, providing us a good starting point from which we can push our knowledge further.

We start with introducing the necessary formalism in chapter one. After a brief summary of some of the main results of scattering theory, we elaborate a bit more on Freshbach-Fano projection operator formalism. Then the whole theory is applied to the decay processes.

In chapter two, we introduce our model of one or two metastable state(s) decaying into a continuum of states. The continuum is bounded from below. We define the coupling under which the process sets in and we develop a semi-analytical formula for the time evolution of the system.

Having the equations in hand, in chapter three we start our study of the system. We will see how the position of the pole of the scattering matrix and the energy of the metastable state affect the time evolution and the spectral line shape. In case of two metastable states, we shall see how they affect each other and we will observe a behaviour known as stabilization effect of resonance and avoided crossing of resonances.

After rigorous study of the theoretical model, we adjust it to a real problem, the neon–helium–neon cluster and the interatomic Coulombic decay. We shall see the time evolution and the spectrum of this trimer prepared in two different states decaying into one final product. We will concentrate on the area where the two resonances cross, comparing the decay rates obtained from the adiabatic elimination of the continuum, from the full time simulation, from direct calculation of the resonant pole position, and from the spectra.

Atomic units are used in the whole thesis unless stated otherwise.

1. Brief Review of Scattering Theory

In this chapter, we introduce the formalism and summarize some of the main results of scattering theory, which will provide us the necessary support for our results later on.

The Schrödinger equation reads

$$\mathbb{H}|\Psi(t)\rangle = i\frac{\partial}{\partial t}|\Psi(t)\rangle, \tag{1.1}$$

where $|\Psi(t)\rangle$ is time-dependent wave function, $\mathbb{H}$ is Hamiltonian. We split the Hamiltonian into two parts, free Hamiltonian $\mathbb{H}_0$ and potential V,

$$\mathbb{H} = \mathbb{H}_0 + V. \tag{1.2}$$

For the description of the scattering process, the $\mathbb{S}$-matrix operator is introduced. It is defined as an operator that maps the initial state $|i\rangle$ to the final state $|f\rangle$

$$\mathbb{S}(E_i)|i\rangle = |f\rangle, \tag{1.3}$$

where we have assumed that the so-called asymptotic condition is fulfilled, that is, for every $|i\rangle$ there exists $|\Psi(t)\rangle$ such that

$$\lim_{t\to-\infty} \||i\rangle - |\Psi(t)\rangle\| = 0 \tag{1.4}$$

and for every $|f\rangle$ there exists $|\tilde{\Psi}(t)\rangle$ such that

$$\lim_{t\to+\infty} \||f\rangle - |\tilde{\Psi}(t)\rangle\| = 0. \tag{1.5}$$

We define the $\mathbb{S}$-matrix element S_{fi} as

$$S_{fi} = \langle E_i|\mathbb{S}|E_f\rangle\delta(E_f - E_i), \tag{1.6}$$

where $|E_i\rangle$ and $|E_f\rangle$ are eigenfunctions of $\mathbb{H}_0$ with eigenvalues E_i and E_f, $\delta(\cdot)$ is Dirac delta distribution.

The $\mathbb{S}$-matrix operator can be decomposed into two parts, a unit matrix and the $\mathbb{T}$-matrix

$$S_{fi} = \delta_{fi} - 2\pi i\delta(E_f - E_i)T_{fi}, \tag{1.7}$$

where

$$T_{fi} = \langle E_i|V|E_f\rangle, \tag{1.8}$$

δ_{fi} is the Kronecker delta.

For a single-channel scattering problem, the $\mathbb{S}$-matrix attains simple scalar form

$$\mathbb{S}(E) = e^{-2i\delta(E)}, \tag{1.9}$$

where $\delta(E)$ is the phase shift.

1.1 Resonances

Resonances are recognizable by a rapid change in the phase shift and are closely related to the poles E_{res} of the scattering matrix $\mathbb{S}$ (or equivalently $\mathbb{T}$) in complex energy plane E or equivalently k_{res} in the complex momentum plane.

The theory can be developed either in terms of E or k, changing from one to the other by simple substitution $E \leftrightarrow \frac{k^2}{2}$. We will carry out the theory in both variables for clarity and justification of the following procedure.

As it is well explained in Ref. [1], the complex plane of E has two areas, where the poles of the S-matrix can be found:

$$\begin{cases} \text{bound and virtual states} & Re[E_{res}] < 0 \quad \& \quad Im[E_{res}] = 0 \\ \text{resonant states} & Re[E_{res}] > 0 \quad \& \quad Im[E_{res}] < 0 \end{cases} . \tag{1.10}$$

We need to keep in mind that in our case the potential $V(E)$ in 1.2 will be function of real variable E, thus we will work with analytically continued function of complex variable $V(E)$ that equals the original one on real axis. With this come few problems, mainly the existence of branch cut along the positive real axis, when changing the variable to k. The four areas we obtain from the substitution are

$$\begin{cases} \text{bound states} & Re[k] = 0 \quad \& \quad Im[k] > 0 \\ \text{resonant states I} & Re[k] > 0 \quad \& \quad Im[k] < 0 \\ \text{resonant states II} & Re[k] < 0 \quad \& \quad Im[k] < 0 \\ \text{virtual states} & Re[k] = 0 \quad \& \quad Im[k] < 0 \end{cases} \tag{1.11}$$

The poles of the resonant states have one more quality – they appear in pairs reflecting each other with respect to the imaginary axis [1].

Since we are particularly interested in how the time evolution of the resonant wave function is affected by poles of $\mathbb{S}$-matrix, we need to develop a consistent and solid procedure of finding their position. This task has been already done by so-called Freshbach-Fano projection operator formalism [2].

1.2 Freshbach-Fano Projection Operator Formalism

The key idea of Freschbach-Fano formalism is to split the Hilbert space $\mathscr{H}$ into two subspaces, the so-called background scattering subspace $\mathscr{P}$ corresponding to slow and smooth changes in phase shift, and the resonant subspace $\mathscr{Q}$ corresponding to rapidly changing phase shift. We require

$$\mathscr{P} \oplus \mathscr{Q} = \mathscr{H}. \tag{1.12}$$

To this end, we define two mutually orthogonal projection operators to these subspaces, $\mathbb{P}$ and $\mathbb{Q}$

$$\mathbb{Q} = \sum_{d=1}^{n} |\varphi_d\rangle\langle\varphi_d|, \tag{1.13}$$

$$\mathbb{P} = \int |E'\rangle\langle E'| \mathrm{d}E', \tag{1.14}$$

where we have assumed that it is possible to describe the resonant part of the wave function by quadratically integrable functions $|\varphi_d\rangle$ and restricted ourselves to one channel scattering. In the same manner, we can rewrite the full wave function $|\Psi(t)\rangle$ as a sum of two parts, i.e.

$$|\Psi(t)\rangle = \sum_{d=1}^{n} a_d(t, E_{\varphi_d})|\varphi_d\rangle + \int b(t, E')|E'\rangle \, \mathrm{d}E', \tag{1.15}$$

where the coefficients $a_d(t, E_{\varphi_d})$, $b(t, E)$ are taken such that the normalization condition

$$|\langle\Psi(t)|\Psi(t)\rangle|^2 = 1 \tag{1.16}$$

is satisfied, E_{φ_d} are the energies of the discrete states,

$$E_{\varphi_d} = \langle\varphi_d|\mathbb{H}|\varphi_d\rangle, \tag{1.17}$$

playing the role of parameters, and the integral runs over all continuum states. It then holds (parameters E_{φ_d} are omitted for brevity)

$$\mathbb{Q}|\Psi(t)\rangle = \sum_{d=1}^{n} a_d(t)\mathbb{Q}|\varphi\rangle = \sum_{d=1}^{n} a_d(t)|\varphi\rangle, \tag{1.18}$$

$$\mathrm{P}|\Psi(t)\rangle = \int b(t, E')\mathbb{P}|E'\rangle \mathrm{d}E' = \int b(t, E')|E'\rangle \mathrm{d}E', \tag{1.19}$$

$$\langle E|\varphi_d\rangle = 0. \tag{1.20}$$

Denoting $\mathbb{H}_{QQ} = \mathbb{Q}\mathbb{H}\mathbb{Q}$, $\mathbb{H}_{PQ} = \mathbb{P}\mathbb{H}\mathbb{Q}$ etc., we can project the Schrödinger equation, obtaining

$$(E - \mathbb{H}_{PP})\,\mathbb{P}|\Psi\rangle = \mathbb{H}_{PQ}\mathbb{Q}|\Psi\rangle, \tag{1.21}$$

$$(E - \mathbb{H}_{QQ})\,\mathbb{Q}|\Psi\rangle = \mathbb{H}_{QP}\mathbb{P}|\Psi\rangle. \tag{1.22}$$

Equation 1.21 can be formally solved with respect to the $\mathscr{P}$-component, yielding

$$\mathbb{P}|\Psi\rangle = |E\rangle + (E - \mathbb{H}_{PP} + i\epsilon)^{-1}\,\mathbb{H}_{PQ}\mathbb{Q}|\Psi\rangle, \tag{1.23}$$

where ϵ is an infinitesimal positive parameter, and the term $|E\rangle$ is homogeneous solution to the background scattering problem

$$(E - \mathbb{H}_{PP})|E\rangle = 0. \tag{1.24}$$

Inserting 1.23 into 1.22, we obtain

$$\mathbb{Q}|\Psi\rangle = \left[E - \mathbb{H}_{QQ} - \mathbb{H}_{QP}\,(E - \mathbb{H}_{PP} + i\epsilon)^{-1}\,\mathbb{H}_{PQ}\right]^{-1}\mathbb{H}_{QP}|E\rangle. \tag{1.25}$$

The operator $E - \mathbb{H}_{QQ} - \mathbb{H}_{QP}\,(E - \mathbb{H}_{PP} + i\epsilon)^{-1}\,\mathbb{H}_{PQ}$ has a unique inversion, since it has no real eigenvalues for positive energy.

To proceed further, we split the $\mathbb{T}$-matrix into two parts, the background and the resonant one

$$\mathbb{T} = \mathbb{T}_{bg} + \mathbb{T}_{res}. \tag{1.26}$$

We also rewrite Hamiltonian in three parts, the kinetic term $\mathbb{K}$ and two potentials $\mathbb{H}_{PP} - \mathbb{K}$ and $\mathbb{H} - \mathbb{H}_{PP}$

$$\mathbb{H} = \mathbb{K} + (\mathbb{H}_{PP} - \mathbb{K}) + (\mathbb{H} - \mathbb{H}_{PP}) \,. \tag{1.27}$$

Defining the Green's function of an operator $\mathbb{X}$, $G_{\mathbb{X}}(E)$, and rewriting Schrödinger equation for $|E\rangle$ and $|\Psi\rangle$ in form of Lippmann-Schwinger equation

$$\mathbb{K}|k\rangle = \frac{k^2}{2}|k\rangle, \tag{1.28a}$$

$$\mathbb{H}_{PP}|E\rangle = E|E\rangle \quad \Leftrightarrow \quad |E\rangle = |k\rangle + G_{\mathbb{K}}(E)\,(\mathbb{H}_{PP} - \mathbb{K})\,|E\rangle, \tag{1.28b}$$

$$\mathbb{H}|\Psi\rangle = E|\Psi\rangle \quad \Leftrightarrow \quad |\Psi\rangle = |E\rangle + G_{PP}(E)\,(\mathbb{H} - \mathbb{H}_{PP})\,|\Psi\rangle, \tag{1.28c}$$

we obtain formula for the two parts of $\mathbb{T}$-matrix (also known as two-potential formula, see [1])

$$\mathbb{T}_{bg} = \langle k|\,(\mathbb{H}_{PP} - \mathbb{K})\,|E\rangle, \tag{1.29a}$$

$$\mathbb{T}_{res} = \langle E|\,(\mathbb{H} - \mathbb{H}_{PP})\,|\Psi\rangle = \langle E|\mathbb{H}_{PQ}|\Psi\rangle. \tag{1.29b}$$

Using equation 1.25, equation 1.29b can be explicitly rewritten

$$\mathbb{T}_{res} = \langle E|\mathbb{H}_{PQ}\left[E - \mathbb{H}_{QQ} - \mathbb{H}_{QP}\,(E - \mathbb{H}_{PP} + i\epsilon)^{-1}\,\mathbb{H}_{PQ}\right]^{-1}\mathbb{H}_{QP}|E\rangle, \tag{1.30}$$

providing us with formula for the poles E_{res} of the $\mathbb{S}$-matrix

$$\det\left[E_{res} - \mathbb{H}_{QQ} - \mathbb{H}_{QP}(E_{res} - \mathbb{H}_{PP} + i\epsilon)^{-1}\mathbb{H}_{PQ}\right] = 0. \tag{1.31}$$

Defining (equation 1.17 is written again for comprehensiveness)

$$E_{\varphi_d} = \langle\varphi_d|\mathbb{H}|\varphi_d\rangle, \tag{1.32}$$

$$V_d(E) = \langle\varphi_d|\mathbb{H}|E\rangle, \tag{1.33}$$

$$E = \langle E|\mathbb{H}|E\rangle, \tag{1.34}$$

and taking all other elements of $\mathbb{H}$ equal to zero, we can further simplify equation 1.31 by introducing the complex level shift function

$$F_{ij}(E) = \langle\varphi_i|\mathbb{H}_{QP}\,(E - \mathbb{H}_{PP} + i\epsilon)^{-1}\,\mathbb{H}_{PQ}|\varphi_j\rangle, \;\; i,j = 1,...,n \tag{1.35}$$

where n is the number of discrete states. Using spectral representation of Green's function

$$(E - \mathbb{H}_{PP} + i\epsilon)^{-1} = \int \mathrm{d}E' \frac{|E'\rangle\langle E'|}{E - E' + i\epsilon} \tag{1.36}$$

and recalling the well-known result from theory of distributions

$$\frac{1}{x + i\epsilon} = v.p.\frac{1}{x} - i\pi\delta(x), \tag{1.37}$$

where $v.p.$ denotes principle value integration, the level shift function can be expressed as

$$F_{ij}(E) = \Delta_{ij}(E) - \frac{i}{2}\Gamma_{ij}(E), \tag{1.38}$$

where $\Delta_{ij}(E)$ and $\Gamma_{ij}(E)$ are level shift and resonance width respectively. They are given by

$$\Gamma_{ij}(E) = 2\pi V_i(E)^* V_j(E), \tag{1.39}$$

$$\Delta_{ij}(E) = \frac{1}{2\pi} v.p. \int \frac{\Gamma_{ij}(E')}{E - E'} \mathrm{d}E'. \tag{1.40}$$

Thus the problem of finding the position of the resonance pole of the $\mathbb{S}$-matrix is reduced to solving

$$\det \left[E_{\varphi_i} \delta_{ij} + F_{ij}(E_{res}) - E_{res} \delta_{ij} \right] = 0 \tag{1.41}$$

for n different E_{res}.

If we want to work in k representation, we simply replace E with $k^2/2$ in all equations, leading to

$$\Gamma_{ij}(k) = 2\pi V_i^* \left(\frac{k^2}{2} \right) V_j^* \left(\frac{k^2}{2} \right), \tag{1.42}$$

$$\Delta_{ij}(k) = \frac{1}{2\pi} v.p. \int \frac{\Gamma_{ij}(E')}{\frac{k^2}{2} - E'} \mathrm{d}E', \tag{1.43}$$

$$F_{ij}(k) = \Delta_{ij}(k) - \frac{i}{2} \Gamma_{ij}(k), \tag{1.44}$$

with the resonance pole k_{res} in the k-plane given by

$$\det \left[E_{\varphi_i} \delta_{ij} + F_{ij} \left(\frac{k_{res}^2}{2} \right) - \frac{k_{res}^2}{2} \delta_{ij} \right] = 0 \tag{1.45}$$

1.3 Decay Processes

The theory above has one important application - the decay processes. From now on, we will assume that the system is prepared at $t = 0$ in one of the discrete states (labelled $d = 1$)

$$|\Psi(t = 0)\rangle = |\varphi_1\rangle. \tag{1.46}$$

Using the results we obtained from the scattering theory, we shall study the time evolution of the discrete state $|\varphi_1\rangle$ decaying into the continuum $|E\rangle$.

The main quantities concerning us are the time evolution of the probability of finding the system in $|\varphi_d\rangle$ or $|E\rangle$, given by

$$|\langle \varphi_d | \Psi(t) \rangle|^2 = |a_d(t, E_{\varphi_d})|^2 \tag{1.47}$$

and

$$|\langle E | \Psi(t) \rangle|^2 = |b(t, E)|^2. \tag{1.48}$$

The spectrum $|b(t \to \infty, E)|^2$ can be usually easily obtained experimentally by simply measuring the energies of the products of the decay process.

1.3.1 Fano Model

Fano model is a simple theory describing decay of one discrete state (leaving out index d) $|\varphi\rangle$ into the continuum $|E\rangle$, coupled together with a constant coupling $V = \langle\varphi|\mathbb{H}|E\rangle = c$. This model presupposes that the continuum extends over the interval $(-\infty, \infty)$.

The whole theory is carried out in great detail in [3]. Here we present only the main result. The probability 1.47 is purely exponential, i.e.

$$|a(t)|^2 = \exp(-\Gamma t), \tag{1.49}$$

Γ being the decay rate of the process. The analytical solution gives [3]

$$\Gamma = 2\pi c^2. \tag{1.50}$$

1.3.2 Generalized Fano Model

The coupling between the discrete state and the continuum states, $V = V(E)$, is in general case a function of variable E. We will always assume $V(E)$ to be a real function, but since we will integrate in the complex plane, we need to keep the formalism as if it were a complex function.

Using the form of the wave function 1.15 for only one discrete state, inserting it together with 1.32, 1.33, and 1.34 in 1.1, and taking scalar product with $|\varphi\rangle$ and $|E\rangle$ leads to a set of differential equations for unknown coefficients $a(t)$ and $b(E,t)$

$$i\frac{\mathrm{d}a(t)}{\mathrm{d}t} = E_\varphi a(t) + \int \mathrm{d}E' b(t,E')V(E'), \tag{1.51a}$$

$$i\frac{\mathrm{d}b(t,E)}{\mathrm{d}t} = a(t)V^*(E) + b(E,t)E, \tag{1.51b}$$

with initial condition (see 1.46)

$$a(t=0) = 1,\ b(t=0,E). \tag{1.52}$$

In the limit of energy independent coupling, the probability $|a(t)|^2$ should converge to 1.49.

1.3.3 Deviations from Exponential Decay

The exponential decay 1.49 is predicted from analytical solution for purely constant coupling $V(E)$ and $E \in (-\infty, \infty)$. However, realistic Hamiltonians have spectrum bounded from below.

Let us assume that the continuum runs only over interval (E_{min}, ∞). The coupling $V(E)$ is then separated into two parts, namely

$$V = \begin{cases} V(E) & E > E_{min} \\ 0 & E < E_{min} \end{cases}. \tag{1.53}$$

It can be shown [4] that only by mathematical properties such as imposing 1.16 the introduction of threshold in fact causes deviations from the exponential decay.

Short Times

For very short times, the exponential function 1.49 is in fact the lower constraint for the time evolution of $|a(t)|^2$

$$|a(t)|^2 > \exp(-\Gamma t). \tag{1.54}$$

Long Times

The limit of long times leads to a different result; $|a(t)|^2$ exhibits power law behaviour

$$|a(t)|^2 \sim t^{-n}, \tag{1.55}$$

for a certain n, and is thus always larger than $\exp(-\Gamma t)$ for sufficiently large t.

The time interval where the exponential decay is valid is given (for our case of s-wave) by [4]

$$e^{-\frac{1}{2}\Gamma t} \gg \frac{1}{4\sqrt{\pi}} \frac{\Gamma t^{-3/2}}{\left((E_r - E_{min})^2 + \frac{1}{4}\Gamma^2\right)^{5/4}}, \tag{1.56}$$

where E_r and Γ are energy and width associated with the resonance respectively (given by equation 1.41) and E_{min} is the threshold position. When the left hand side of 1.56 becomes comparable to the right hand side, the decay behaves according to 1.55.

1.3.4 Spectral Line Shape

Now we elaborate a bit more on the problem of the decay spectrum, i.e. the population of states $|E\rangle$ given by

$$|\langle E|\Psi(t)\rangle|^2 = |b(t,E)|^2, \;\; t \to \infty \tag{1.57}$$

The resulting function $|b(E)|^2$ is called the spectral line. It is a well-known fact [5] that if the energy of the decaying state is far above the threshold and the decay is exponential, i.e. 1.49 holds, we can expect the line shape close to Lorentzian curve

$$|b(E)|^2 \cong \frac{\frac{\Gamma_s}{2}}{(E - E_s)^2 + \left(\frac{\Gamma_s}{2}\right)^2}, \tag{1.58}$$

where Γ_s is the decay rate and E_s is the energy of the decaying state. In the ideal case $\Gamma_s = \Gamma(E_{res})$ and $E_s = \Delta(E_{res}) + E_\varphi$, where $\Gamma(E_{res})$ and $\Delta(E_{res})$ are already introduced in equations 1.39 and 1.40.

Note that the result 1.58 is time-independent and therefore well suited for experimentalists.

2. The Model

In the previous chapter, we obtained theoretical description of resonances and poles associated with them. We can now apply the theory on a suitable model.

The equations 2.8 or 2.9 have still one undefined part – the potentials $V_i(E)$. We take all of the potentials in the same form

$$V_i(E) = \begin{cases} \sqrt{\frac{A_i}{2\pi}\frac{E}{B_i}\exp\left(-\frac{E}{B_i}\right)} & E > 0 \\ 0 & E < 0 \end{cases}, \tag{2.1}$$

where A_i and B_i are parameters of i-th coupling. This form was chosen such that it is similar to real cases and is continuous. Moreover, using gamma function $\Gamma(\cdot)$, incomplete gamma function $\Gamma(\cdot,\cdot)$, and confluent hypergeometric function ${}_1F_1(\cdot,\cdot,\cdot)$, we can rewrite the level shift function $F(k)$ in terms of variable $k^2/2 = E$ [6]

$$F_{ij}(k) = -\frac{A_{ij}}{2\pi}\Gamma(2)\frac{-k^2}{2B_{ij}}\Gamma\left(-1,-\frac{k^2}{2B_{ij}}\right)\exp\left(-\frac{k^2}{2B_{ij}}\right), \tag{2.2}$$

where

$$A_{ij} = 2\frac{\sqrt{A_iA_jB_iB_j}}{B_i+B_j} \tag{2.3}$$

and

$$B_{ij} = 2\frac{B_iB_j}{B_i+B_j}. \tag{2.4}$$

The formula 2.2 is valid on real axis, but since all functions are meromorphic, it can be straightforwardly continued to the complex k-plane.

We can now search for the positions of the poles of the $\mathbb{S}$-matrix operator as a function of one of the parameters A_i, B_i or E_{φ_i}. Let us choose E_{φ_1}. The way to find the positions of the poles is straightforward. We fix all the parameters in such a way that the coupling near E_{φ_1} is very small. Therefore we can use first order perturbation theory to approximate $E_{res_i} \cong E_{\varphi_i} - \frac{i}{2}\Gamma_i^{1PT}$ with (see [3])

$$\Gamma_i^{1PT} = 2\pi|V(E_{\varphi_i})|^2. \tag{2.5}$$

This equation is only valid for the probability 1.47 that can be well-approximated by exponential function. Setting

$$k_{approx_i} = \sqrt{2\left(E_{\varphi_i} - \frac{i}{2}\Gamma_i^{1PT}\right)}, \tag{2.6}$$

we acquire an approximate position of the pole. We can search for the k_{res_i} in the vicinity of k_{approx_i}. Changing one of the parameters slightly, we obtain the pole position as a function of this parameter, using always the previous position as a starting point, since the approximation 2.6 does not have to be valid any more (see figure 2.1).

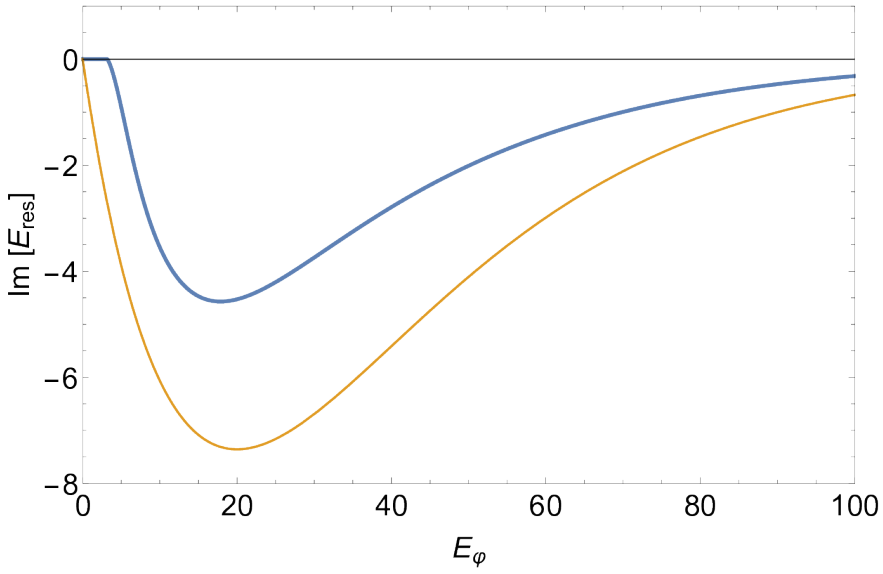

Figure 2.1: An example of a deviation of the first order perturbation theory 2.5 (yellow curve) from the actual imaginary part of the pole position (blue curve). The system has only one discrete state with coupling 2.1 defined by parameters $A = A_1 = 20$ and $B = B_1 = 20$.

2.1 Isolated Resonance

In the case of only one discrete state $|\varphi\rangle$, the Hamiltonian is

$$\mathbb{H} = \left(\begin{array}{c|ccc} E_\varphi & & V(E) & \\ \hline & \ddots & & 0 \\ V^*(E) & & E & \\ & 0 & & \ddots \end{array}\right), \tag{2.7}$$

given in basis of $|\varphi\rangle$ and $|E\rangle$. Note, that this Hamiltonian satisfies 1.32 – 1.34. The equations 1.41 and 1.45 reduce to

$$E_\varphi + F(E_{res}) - E_{res} = 0, \tag{2.8}$$

$$E_\varphi + F(k_{res}) - \frac{k_{res}^2}{2} = 0. \tag{2.9}$$

2.2 Two Resonances

The case of two resonances leads to a wave function of the form

$$|\Psi(t)\rangle = a_1(t, E_{\varphi_1})|\varphi_1\rangle + a_2(t, E_{\varphi_2})|\varphi_2\rangle + \int b(t, E')|E'\rangle \, \mathrm{d}E', \tag{2.10}$$

with the Hamiltonian in the basis of discrete and continuum states

$$\mathbb{H} = \left(\begin{array}{cc|c} E_{\varphi_1} & 0 & V_1(E) \\ \hline 0 & E_{\varphi_2} & V_2(E) \\ \hline & & \ddots \quad 0 \\ V_1^*(E) & V_2^*(E) & \quad E \\ & & 0 \quad \ddots \end{array}\right). \tag{2.11}$$

The system of differential equations 1.51 becomes

$$i\frac{\mathrm{d}a_1(t)}{\mathrm{d}t} = E_{\varphi_1}a_1(t) + \int \mathrm{d}E' b(t,E')V_1(E'), \tag{2.12a}$$

$$i\frac{\mathrm{d}a_2(t)}{\mathrm{d}t} = E_{\varphi_2}a_2(t) + \int \mathrm{d}E' b(t,E')V_2(E'), \tag{2.12b}$$

$$i\frac{\mathrm{d}b(t,E)}{\mathrm{d}t} = a_1(t)V_1^*(E) + a_2(t)V_2^*(E) + b(t,E)E. \tag{2.12c}$$

The level shift function is now matrix 2x2 and the positions of the poles are given by full equation 1.41 or 1.45.

2.2.1 Adiabatic Elimination of the Continuum

We may now try to solve the system 2.12 explicitly. Following the procedure in [7, 8, 9], we substitute

$$a_1 \to a_1\, e^{-iE_{\varphi_1}t}, \tag{2.13a}$$

$$a_2 \to a_2\, e^{-iE_{\varphi_2}t}, \tag{2.13b}$$

$$b \to b\, e^{-iEt} \tag{2.13c}$$

into equations 2.12, simplifying 2.12 to

$$i\frac{\mathrm{d}a_1(t)}{\mathrm{d}t} = \int \mathrm{d}E' b(t,E')V_1(E')e^{-i\left(E'-E_{\varphi_1}\right)t}, \tag{2.14a}$$

$$i\frac{\mathrm{d}a_2(t)}{\mathrm{d}t} = \int \mathrm{d}E' b(t,E')V_2(E')e^{-i\left(E'-E_{\varphi_2}\right)t}, \tag{2.14b}$$

$$i\frac{\mathrm{d}b(t,E)}{\mathrm{d}t} = a_1(t)V_1^*(E)e^{-i\left(E_{\varphi_1}-E'\right)t} + a_2(t)V_2^*(E)e^{-i\left(E_{\varphi_2}-E'\right)t}. \tag{2.14c}$$

Since we know $b(0,E) = 0$, we can formally integrate 2.14c

$$b(t,E) = -i\int_{-\infty}^{t} \mathrm{d}\tau\, \Theta(\tau)\left[a_1(\tau)V_1^*(E)e^{-i\left(E_{\varphi_1}-E\right)\tau} + a_2(\tau)V_2^*(E)e^{-i\left(E_{\varphi_2}-E\right)\tau}\right], \tag{2.15}$$

where $\Theta(\cdot)$ is Heaviside theta distribution. This distribution is introduced to ensure that $a_1(t<0) = 0$, $a_2(t<0) = 0$, and $b(t<0,E) = 0$.

Substituting 2.15 into 2.14a and 2.14b leads to two integro-differential equa-

tions

$$\frac{\mathrm{d}a_1(t)}{\mathrm{d}t} = -\int \mathrm{d}E' V_1(E') e^{-i\left(E'-E_{\varphi_1}\right)t} \times \int_{-\infty}^{t} \mathrm{d}\tau\, \Theta(\tau) \left[a_1(\tau) V_1^*(E') e^{-i\left(E_{\varphi_1}-E'\right)\tau} + a_2(\tau) V_2^*(E') e^{-i\left(E_{\varphi_2}-E'\right)\tau}\right]. \tag{2.16a}$$

$$\frac{\mathrm{d}a_2(t)}{\mathrm{d}t} = -\int \mathrm{d}E' V_2(E') e^{-i\left(E'-E_{\varphi_2}\right)t} \times \int_{-\infty}^{t} \mathrm{d}\tau\, \Theta(\tau) \left[a_1(\tau) V_1^*(E') e^{-i\left(E_{\varphi_1}-E'\right)\tau} + a_2(\tau) V_2^*(E') e^{-i\left(E_{\varphi_2}-E'\right)\tau}\right]. \tag{2.16b}$$

For convergence reasons, we multiply the integrand under the time integral with $1 = e^{\eta\tau-\eta\tau}$. In the end we take the limit $\eta \to 0$. We will rewrite the part under the time integral and take the Taylor expansion near the point $t = \tau > 0$

$$\begin{aligned} &\left[\Theta(\tau) a_i(\tau) e^{-\eta\tau}\right] e^{-i\left(E_{\varphi_i}-E'\right)\tau+\eta\tau} \\ &= \left[a_i(t) + \left.\frac{\mathrm{d}a_i(\tau)}{\mathrm{d}\tau}\right|_{\tau=t} (t-\tau) - \eta a_i(t)(t-\tau) + a_i(t)\delta(t)(t-\tau)\right] \\ &\quad \times e^{-\eta t} e^{-i\left(E_{\varphi_i}-E'\right)\tau+\eta\tau}. \end{aligned} \tag{2.17}$$

The term with Dirac distribution $\delta(\cdot)$ in 2.17 represents the discontinuity of $a_{1,2}(t)$ as a function of time at time $t = 0$. We will not consider this term in the following because it is almost everywhere zero. The third term in 2.17 disappears when taking the limit $\eta \to 0$, leaving us with first and second term. The second term after integrating per-partes over τ gives contribution of the form

$$\dot{a_i}(t) \int_0^\infty \mathrm{d}E' \frac{V_i^*(E') V_j(E')}{\left(E_{\varphi_i} - E' + i\eta\right)^2}. \tag{2.18}$$

The integral can be calculated explicitly using the exponential integral function for the couplings 2.1. We will not give the whole formula as it has long and complicated form. Both real and imaginary part of the integral in 2.18 becomes of order 10^{-1} around $E_{\varphi_i} > 80$ and of order 10^{-2} around $E_{\varphi_i} > 120$ for $E_{\varphi_1} = 100$, $A_1 = 20$, $A_2 = 30$, and $B_1 = B_2 = 20$. These will be the parameters we use later on. For these parameters, we can neglect the second term in 2.17 since on the left hand side of system 2.16 is the derivative $\dot{a}_i(t)$ with coefficient one. For area $E_{\varphi_i} < 80$, we have to use numerical integration of equations 2.12 to find the time evolution of the system.

The first term in the bracket in 2.17 after integrating over τ gives

$$\begin{aligned} \frac{\mathrm{d}a_1(t)}{\mathrm{d}t} &= -ia_1(t) \int \mathrm{d}E' V_1(E') V_1^*(E') \frac{1}{E_{\varphi_1} - E' + i\eta} \\ &\quad - ia_2(t) \int \mathrm{d}E' V_1(E') V_2^*(E') \frac{1}{E_{\varphi_2} - E' + i\eta} e^{i\left(E_{\varphi_1}-E_{\varphi_2}\right)t}, \end{aligned} \tag{2.19a}$$

$$\begin{aligned} \frac{\mathrm{d}a_2(t)}{\mathrm{d}t} &= -ia_1(t) \int \mathrm{d}E' V_2(E') V_1^*(E') \frac{1}{E_{\varphi_1} - E' + i\eta} e^{-i\left(E_{\varphi_1}-E_{\varphi_2}\right)t} \\ &\quad - ia_2(t) \int \mathrm{d}E' V_2(E') V_2^*(E') \frac{1}{E_{\varphi_2} - E' + i\eta}. \end{aligned} \tag{2.19b}$$

The integral

$$I_{klm} = \int \mathrm{d}E' V_k(E') V_l^*(E') \frac{1}{E_{\varphi_m} - E' + i\eta} \tag{2.20}$$

can be calculated explicitly for couplings 2.1. Note that in fact (recalling 1.37)

$$I_{klm} = \Delta_{kl}(E_{\varphi_m}) - \frac{i}{2}\Gamma_{kl}(E_{\varphi_m}) \tag{2.21}$$

as defined above. Using notation 2.20, the system 2.19 boils down to

$$\frac{\mathrm{d}a_1(t)}{\mathrm{d}t} = -\,i\left[a_1(t) I_{111} + a_2(t) I_{122}\, e^{i\left(E_{\varphi_1} - E_{\varphi_2}\right)t}\right], \tag{2.22a}$$

$$\frac{\mathrm{d}a_2(t)}{\mathrm{d}t} = -\,i\left[a_1(t) I_{211}\, e^{-i\left(E_{\varphi_1} - E_{\varphi_2}\right)t} + a_2(t) I_{222}\right]. \tag{2.22b}$$

This system can be rewritten as

$$\begin{pmatrix} \dot{a_1} \\ \dot{a_2} \end{pmatrix} = -i \begin{pmatrix} I_{111} & I_{122}\, e^{i\left(E_{\varphi_1} - E_{\varphi_2}\right)t} \\ I_{211}\, e^{-i\left(E_{\varphi_1} - E_{\varphi_2}\right)t} & I_{222} \end{pmatrix} \begin{pmatrix} a_1 \\ a_2 \end{pmatrix}, \tag{2.23}$$

with eigenvalues

$$I_{\pm} = -\frac{i}{2}\left(I_{111} + I_{222} \pm \sqrt{\left(I_{111} - I_{222}\right)^2 + 4 I_{122} I_{211}}\right). \tag{2.24}$$

The eigenvectors

$$R_1 = \left(e^{2i\left(E_{\varphi_1} - E_{\varphi_2}\right)t} \frac{I_{111} - I_{222} + \sqrt{\left(I_{111} - I_{222}\right)^2 + 4 I_{122} I_{211}}}{2 I_{211}}, 1\right). \tag{2.25a}$$

$$R_2 = \left(e^{2i\left(E_{\varphi_1} - E_{\varphi_2}\right)t} \frac{I_{111} - I_{222} - \sqrt{\left(I_{111} - I_{222}\right)^2 + 4 I_{122} I_{211}}}{2 I_{211}}, 1\right) \tag{2.25b}$$

are not orthogonal in general. They become orthogonal for either real $V(E)$ and $E_{\varphi_1} = E_{\varphi_2}$ (note that in this case $I_{122} = I_{211}$) or for E_{φ_1} and E_{φ_2} far away form each other. In the second case, $I_{122} = I_{211} \cong 0$ and the matrix 2.23 is therefore diagonal. The resonances then do not influence each other. The imaginary parts of the eigenvalues $I_{\pm}$ provide approximations to the decay widths of the two resonances.

$$\Gamma_{\pm} = 2Im\left[I_{\pm}\right]. \tag{2.26}$$

The precise decay width Γ of the discrete state can be determined by solving 2.23, which can be done numerically. It should be noted that even in case when one isolated resonance decays exponentially, when second resonance is added into the system, the solution of 2.23 is not necessarily exponential decay any more. The resonances influence each other leading to modification in the decay such as oscillations of probability 1.47.

3. Results and Discussion

Now we have full theoretical description of the system; let us just summarize the results we obtained. The couplings of the system are

$$V_i(E) = \begin{cases} \sqrt{\frac{A_i}{2\pi}\frac{E}{B_i}\exp\left(-\frac{E}{B_i}\right)} & E > 0 \\ 0 & E < 0 \end{cases}, \tag{3.1}$$

which reduces for one discrete state to

$$V(E) = \begin{cases} \sqrt{\frac{A}{2\pi}\frac{E}{B}\exp\left(-\frac{E}{B}\right)} & E > 0 \\ 0 & E < 0 \end{cases} \tag{3.2}$$

The position of the poles of the $\mathbb{S}$-matrix operator is given by

$$\det\left[E_{\varphi_i}\delta_{ij} + \mathbb{F}(E_{res}) - E_{res}\delta_{ij}\right] = 0, \tag{3.3}$$

or

$$\det\left[E_{\varphi_i}\delta_{ij} + \mathbb{F}\left(\frac{k_{res}^2}{2}\right) - \frac{k_{res}^2}{2}\delta_{ij}\right] = 0. \tag{3.4}$$

For only one resonance, it reduces to

$$E_\varphi + F(E_{res}) - E_{res} = 0, \tag{3.5}$$

$$E_\varphi + F(k_{res}) - \frac{k_{res}^2}{2} = 0. \tag{3.6}$$

We have two formulae for the time evolution of $a_i(t)$, namely the numerical solution of 1.51 for one resonance or 2.12 for two resonances and the semi-analytical formula given by the solution of 2.23. The decay spectrum is given by

$$|b(E)|^2 \cong \frac{\frac{\Gamma_s}{2}}{(E - E_s)^2 + \left(\frac{\Gamma_s}{2}\right)^2}, \tag{3.7}$$

We also have three definitions of Γ: one is twice the imaginary part of the resonance pole position $\Gamma(E_{res})$; then we have the adiabatic elimination approximation $\Gamma_\pm$ – note that for one resonance it reduces to the first order perturbation theory approximation $\Gamma^{1PT} = 2\pi|V(E_\varphi)|^2$; and finally Γ_s given by the spectral line shape.

3.1 One Resonance

In the case of one resonance, we shall study the threshold influence on the time evolution and on the spectrum of the system. We push the discrete state closer to the threshold by making E_φ smaller, fixing at the same time the parameters A and B of the coupling 3.2. We choose these parameters so that we can see a clear transition from resonant to bound state for E_φ sufficiently larger than zero. At the same time, we want to see exponential decay far above the threshold and

therefore we need the coupling there to be large enough so that the discrete state still decays quickly enough. The third demand for the coupling is that it has to be sufficiently close to zero around the upper limit of the interval we are able to numerically integrate, that is, we need to be able to make sufficiently dense discretization of the continuum on most of the relevant energy interval (see [10] for more details). For these reasons, we set $A = 20$ and $B = 20$, leaving the position of the poles of the $\mathbb{S}$-matrix operator to be a function of E_φ.

The final smooth curve of the pole positions as a function of E_φ is shown in figures 3.1 (in variable k) and 3.2 (in variable E). Position of the resonant pole in the complex plane is in figures 3.3 and 3.4. The black arrows indicate how the pole moves along the curve with decreasing E_φ.

In correspondence with previously stated (section 1.1), we can see the transition to a bound state at point $E_\varphi = 3.184$, manifesting itself by switching the area

$$Re[k] \gtrless 0 \,\&\, Im[k] < 0 \rightarrow Re[k] = 0 \,\&\, Im[k] \gtrless 0,$$

for k-representation, or

$$Re[E] > 0 \,\&\, Im[E] < 0 \rightarrow Re[E] < 0 \,\&\, Im[E] = 0$$

for E-representation, see 1.11 and 1.10 respectively.

If we look closely at the time evolution (figures 3.5 - 3.13), we can see a clear transition from exponential to polynomial decay, see figures 3.6, 3.7, and 3.8. We should see this transition when the right hand side of 1.56 becomes comparable with the left hand side. For system on figure 3.6 this happen around $t = 2.7$, for system on figure 3.7 around $t = 1.7$, and finally for system on figure 3.8 around $t = 1.6$. So 1.56 gives a reasonable prediction. Note that the transition is always preceded by a characteristic local decrease of $|a(t)|^2$ [4].

When $E_\varphi < 3.184$ (figures 3.12 and 3.13) the discrete state does not decay completely any more. We have to keep in mind that the discrete state is not the resonant state. It is a combination of the resonant state and the continuum states, causing a partial decay of the discrete state even in area where the system has a bound state.

The first order perturbation theory gives us a good prediction in the area far above the threshold and for short times where the decay is exponential (figures 3.5 to 3.8). When the discrete state is pushed near the threshold (figures 3.9 and 3.10), the decay after short time becomes considerably different from the first order perturbation theory. The slope of the line describing the decay process is in fact far closer to Γ_s given by the spectral line shape than to Γ^{1PT}. This fact is logical given that the spectral line is taken in limit for $t \rightarrow \infty$. Fitted value of the slope for system on figure 3.9 is 0.93 ± 0.01 (compare with $\Gamma_s = 1.15 \pm 0.01$ and $\Gamma^{1PT} = 3.89$) and 0.35 ± 0.01 (compare with $\Gamma_s = 52 \pm 0.01$ and $\Gamma^{1PT} = 3.27$) for system on figure 3.10. For short times, the first order perturbation theory is valid for $E_\varphi > 3$ but for $E_\varphi < 3$ it breaks completely – compare detailed figures 3.14, 3.15, and 3.16.

The presence of the threshold also impacts the shape of the Lorentzian-like curve of the spectra. The curve becomes distinctively asymmetric – the states on the right hand side from the centre of the curve are more populated that those on the left hand side (figures 3.7 to 3.9). The threshold also causes the Lorentzian curve to be narrower, which is very well observable from the difference between

the actual Γ_{res}, given by twice the imaginary part of the pole position, and the defining parameter Γ_s of the Lorentzian curve.

Another significant feature are the oscillations on the spectral line shape, which become more pronounced the closer we are to the threshold (figures 3.10 and 3.11), breaking the line shape completely when the resonant state becomes a bound state (figure 3.12 and 3.13). This can be explained by the fact that our discrete state is actually not the resonance state, but a combination of the resonant state and some states from the continuum. The coefficients of the decomposition are in fact the square roots of the population values of each of the continuum state.

3.2 Two Overlapping Resonances

In the very same manner, we shall study the system with two discrete states. We can again find the positions of the poles as functions of one parameter; we choose E_{φ_2}. The coupling 3.1 is used with very similar parameters not only for reasons explained in the previous section, but also to have the opportunity to compare the results with the case of one discrete state in the system. We take E_{φ_1} and E_{φ_2} large enough so that the threshold effect is negligible.

We start by drawing the function of poles positions. We set the parameters $E_{\varphi_1} = 100$, $A_1 = 20$, $A_2 = 30$, and $B_1 = B_2 = 20$. The resulting function of E_{φ_2} is in figures 3.17 and 3.18 for k- and E-representation respectively. The positions of the poles in the complex plain are in figures 3.19 and 3.20 (detailed) for k-representation and 3.21 for E-representation. The black arrows show the poles moving along the curves with increasing E_{φ_2}. The green dot indicates where the pole is when only one resonance associated with $E_{\varphi_1} = 100$ is in the system (compare with figure 3.5). When enlarging E_{φ_2} from $E_{\varphi_2} = 50$, one of the poles starts moving along the yellow curve, while the other one is pushed from the green dot and starts moving along the blue curve. When $E_{\varphi_2} \cong E_{\varphi_1} = 100$ the poles are one above another at position approximately $Re[E_{res}] \cong 100$, but one of the resonances is stabilized (the imaginary part is effectively zero), while the other one decays faster than it would decay if it were an isolated resonance. The stabilization of one of the resonances is called bound state in continuum and is studied in detail in [7, 11]. When enlarging E_{φ_2} even further, the resonance poles "swap their meaning" and the pole originally placed at the green dot moves away while the other one converges to the green dot instead. This is better visible in following figures 3.22 to 3.27.

Swapping the pole correspondence to individual discrete state is also clear from all of the figures 3.17 and 3.18. We see that neither the imaginary part of k_{res_i} nor imaginary part of E_{res_i} of either pole converges to zero on one of the boundaries. They converge to the pole position of the first isolated resonance, that is to $k_{res} = \pm 14.22 - 0.02i$ or $E_{res} = 101.12 - 0.32i$, compare with 3.5. Such behaviour, when one pole continues its trajectory in the complex plane in a way that optically looks like the trajectory of the other one, is called avoided crossing.

The exact time evolution shown in figures 3.22 to 3.27 is well described by the adiabatic elimination of the continuum. Remember we deliberately work in the area where the correction 2.18 is small enough. For these set-ups the decay is (apart from the oscillations caused by the presence of the two discrete states

in the system) purely exponential, no transition to polynomial decay is observed.

Around $E_{\varphi_2} = 100$ (figures 3.24 and 3.25), the stabilization effect comes into play, when one of the poles reaches almost $Im[k_{res}] = 0$, while the other one suddenly acquires $Im[k_{res}]$ far larger. The two discrete states are again a combination of the two resonance states, so the decay is then dominated in the beginning by fast decay from one of the resonances, and then it relaxes into slow decay of the second resonance. In the end, it seems that there is a bound state in the system, far above the area where we expect any bound states – the bound state in continuum effect.

Now let us look at the spectra. Remember that we always start from $|\varphi_1\rangle$, the population of the other discrete state is zero. This causes that the spectrum is mostly populated from the first discrete state with only a small peak stemming from the second one when the discrete states are far from each other (figures 3.22, 3.23, 3.26, and 3.27). This causes large error in the estimate of Γ_s of one of the resonances.

In these areas where the resonances are far from each other, the eigenstates 2.25 are almost orthogonal and

$$|\varphi_1\rangle \cong |R_1\rangle, \tag{3.8}$$

$$|\varphi_2\rangle \cong |R_2\rangle \tag{3.9}$$

but when we push E_{φ_2} closer to E_{φ_1}, the discrete states become

$$|\varphi_1\rangle = \sum_i c_i |R_i\rangle, \ |c_1| \cong |c_2|, \tag{3.10}$$

$$|\varphi_2\rangle = \sum_i c_i |R_i\rangle, \ |c_1| \cong |c_2| \tag{3.11}$$

and therefore the spectrum has two peaks, one from each resonance (figures 3.24 and 3.25). The Γ_s obtained from spectrum of the resonance with larger Γ_{res} is similar to Γ_{res}, whereas Γ_s of the stabilized resonance is completely different. This may be because numerical integration of 2.12 for two close discrete states could not be done for sufficiently large t and therefore the spectrum may not be converged. Either way, the parameter Γ_s is not a good approximation for us in case of two overlapping resonances.

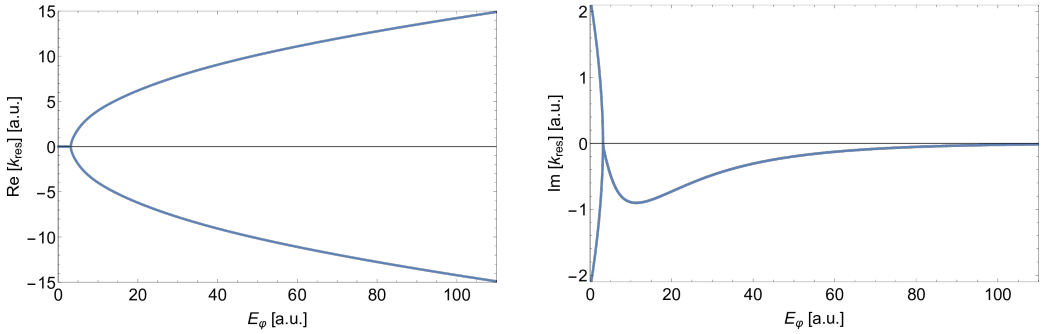

Figure 3.1: Real and imaginary part of the position of the resonant pole k_{res} given by 3.6 as a function of E_φ. The coupling 3.2 is defined by parameters $A = 20$ and $B = 20$.

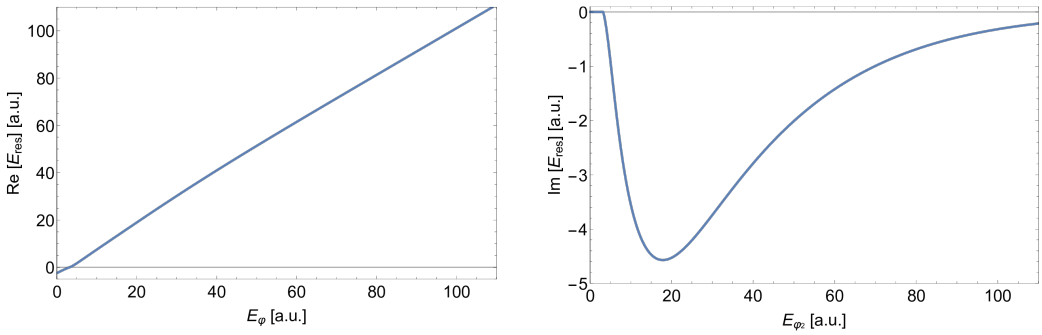

Figure 3.2: Real and imaginary part of the position of the resonant pole E_{res} given by 3.5 as a function of E_φ. The coupling 3.2 is defined by parameters $A = 20$ and $B = 20$.

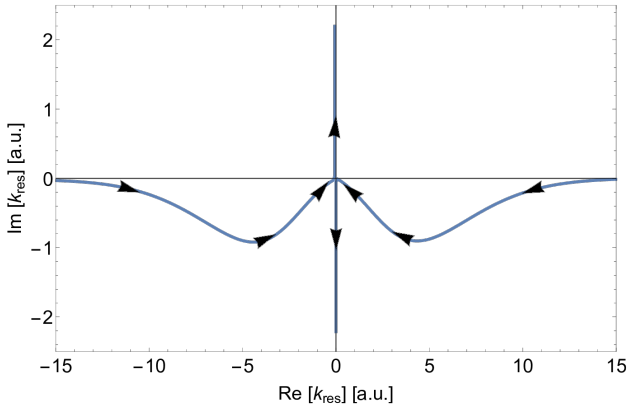

Figure 3.3: Position of the resonant pole k_{res} given by 3.6 as a function of E_φ. The smaller E_φ is, the more the pole approaches point $[0, 0]$ (reaching it at the point $E_\varphi = 3.184$), then it starts moving up or down along the imaginary axis as the bound and virtual state respectively, as the arrows indicate. The coupling 3.2 is defined by $A = 20$ and $B = 20$.

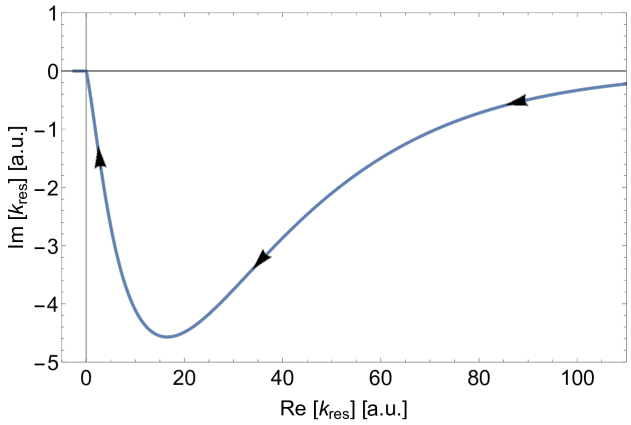

Figure 3.4: The position of the resonant pole E_{res} given by 3.5 as a function of E_φ. The smaller E_φ is, the more the pole approaches point $[0, 0]$ (reaching it at the point $E_\varphi = 3.184$), then it becomes bound state and starts moving along the negative real axis, as the arrows indicate. The coupling 2.1 is defined by $A = 20$ and $B = 20$.

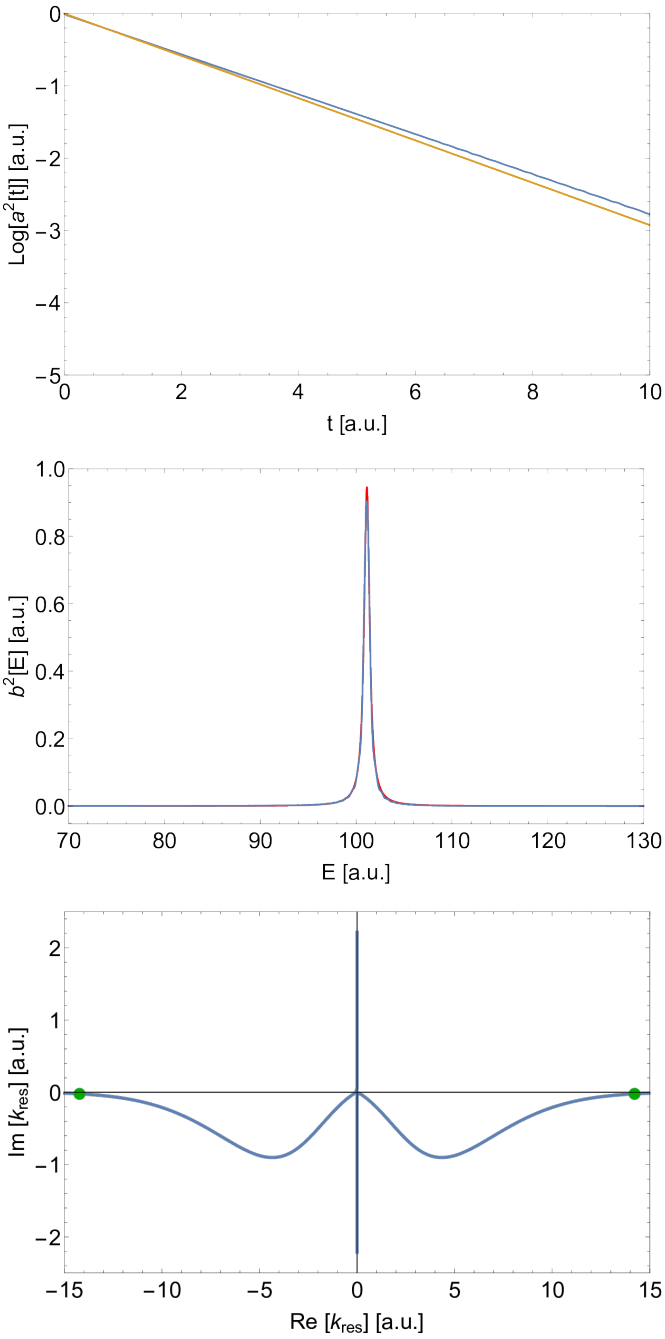

k_{res}	$Re[E_{res}]$	Γ_{res}	Γ^{1PT}	Γ_s	E_s
$\pm 14.22 - 0.02i$	101.12	0.64	0.67	0.68 ± 0.01	101.12 ± 0.01

Figure 3.5: The system is defined by coupling 3.2 with parameters $A = 20$ and $B = 20$, and by position of the discrete state $E_\varphi = 100$.
First: time evolution $|a|^2$ given by 1.51 – blue curve – and first order perturbation prediction 2.5 – yellow curve (in common logarithmic scale). Second: the spectrum $|b|^2$ given by 1.48 – blue curve – fitted with function 3.7 – red curve. Third: the position of the resonant poles (green dots). Fourth: table of parameters and poles positions.

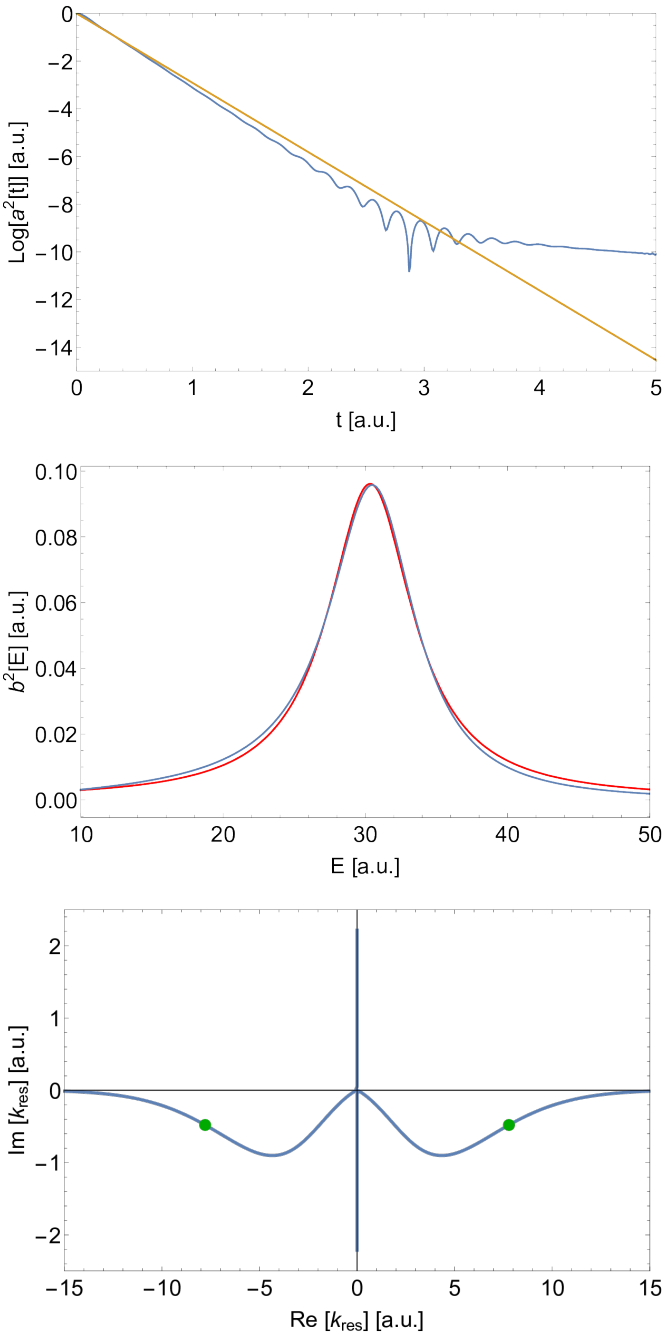

k_{res}	$Re[E_{res}]$	Γ_{res}	Γ^{1PT}	Γ_s	E_s
$\pm 7.78 - 0.48i$	30.18	7.48	6.67	7.17 ± 0.01	30.34 ± 0.1

Figure 3.6: The system is defined by coupling 3.2 with parameters $A = 20$ and $B = 20$, and by position of the discrete state $E_\varphi = 30$.
First: time evolution $|a|^2$ given by 1.51 – blue curve – and first order perturbation prediction 2.5 – yellow curve (in common logarithmic scale). Second: the spectrum $|b|^2$ given by 1.48 – blue curve – fitted with function 3.7 – red curve. Third: the position of the resonant poles (green dots). Fourth: table of parameters and poles positions.

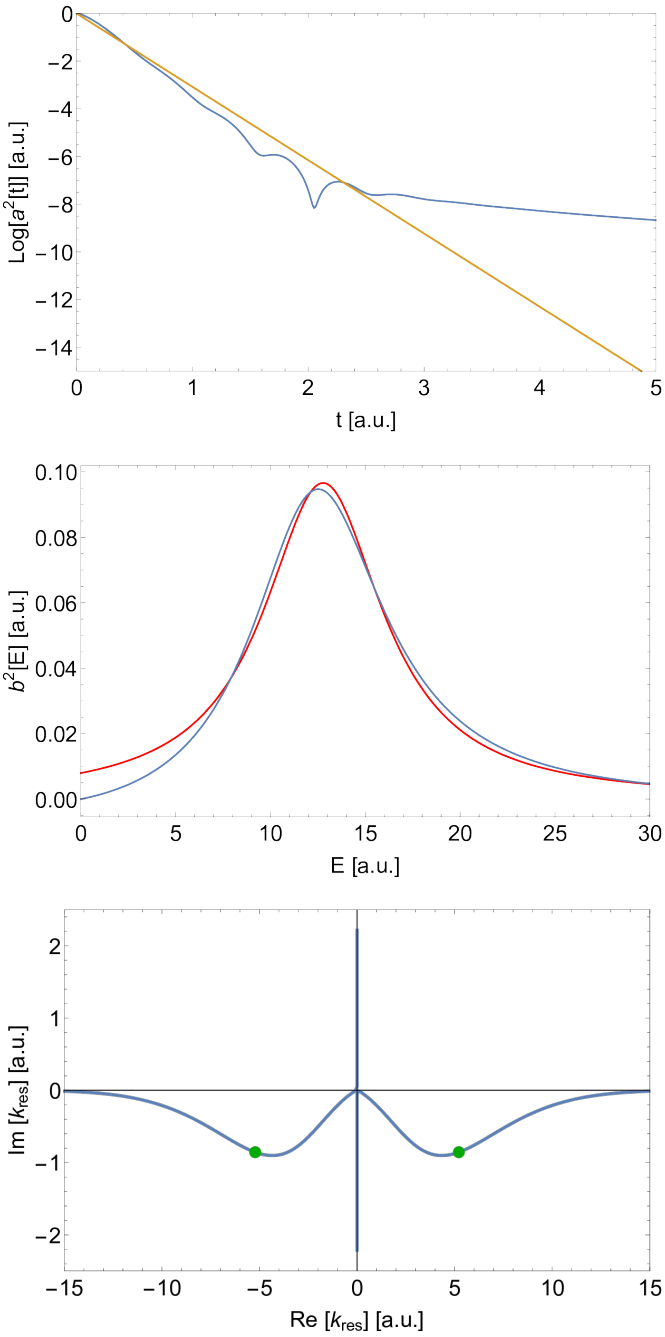

k_{res}	$Re[E_{res}]$	Γ_{res}	Γ^{1PT}	Γ_s	E_s
$\pm 5.21 - 0.83i$	13.22	8.66	7.08	7.65 ± 0.03	12.77 ± 0.1

Figure 3.7: The system is defined by coupling 3.2 with parameters $A = 20$ and $B = 20$, and by position of the discrete state $E_\varphi = 15$.
First: time evolution $|a|^2$ given by 1.51 – blue curve – and first order perturbation prediction 2.5 – yellow curve (in common logarithmic scale). Second: the spectrum $|b|^2$ given by 1.48 – blue curve – fitted with function 3.7 – red curve. Third: the position of the resonant poles (green dots). Fourth: table of parameters and poles positions.

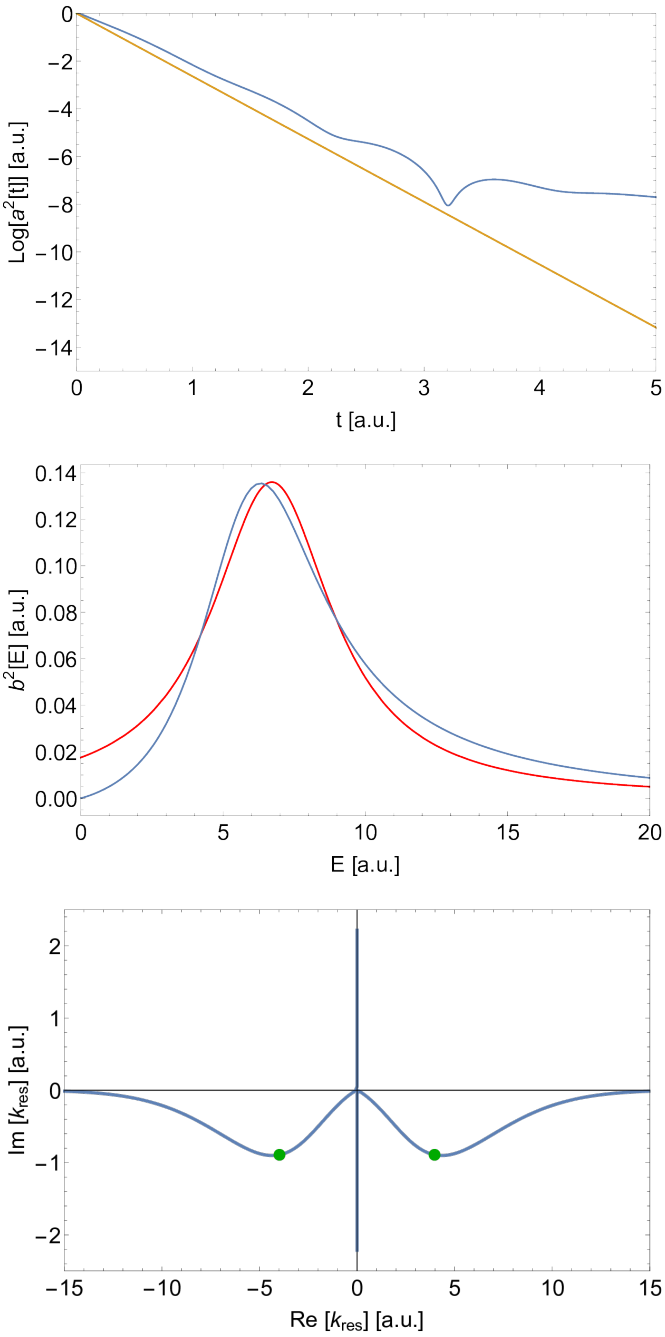

k_{res}	$Re[E_{res}]$	Γ_{res}	Γ^{1PT}	Γ_s	E_s
$\pm 3.97 - 0.89i$	7.49	7.10	6.07	5.16 ± 0.04	6.71 ± 0.1

Figure 3.8: The system is defined by coupling 3.2 with parameters $A = 20$ and $B = 20$, and by position of the discrete state $E_\varphi = 10$.
First: time evolution $|a|^2$ given by 1.51 – blue curve – and first order perturbation prediction 2.5 – yellow curve (in common logarithmic scale). Second: the spectrum $|b|^2$ given by 1.48 – blue curve – fitted with function 3.7 – red curve. Third: the position of the resonant poles (green dots). Fourth: table of parameters and poles positions.

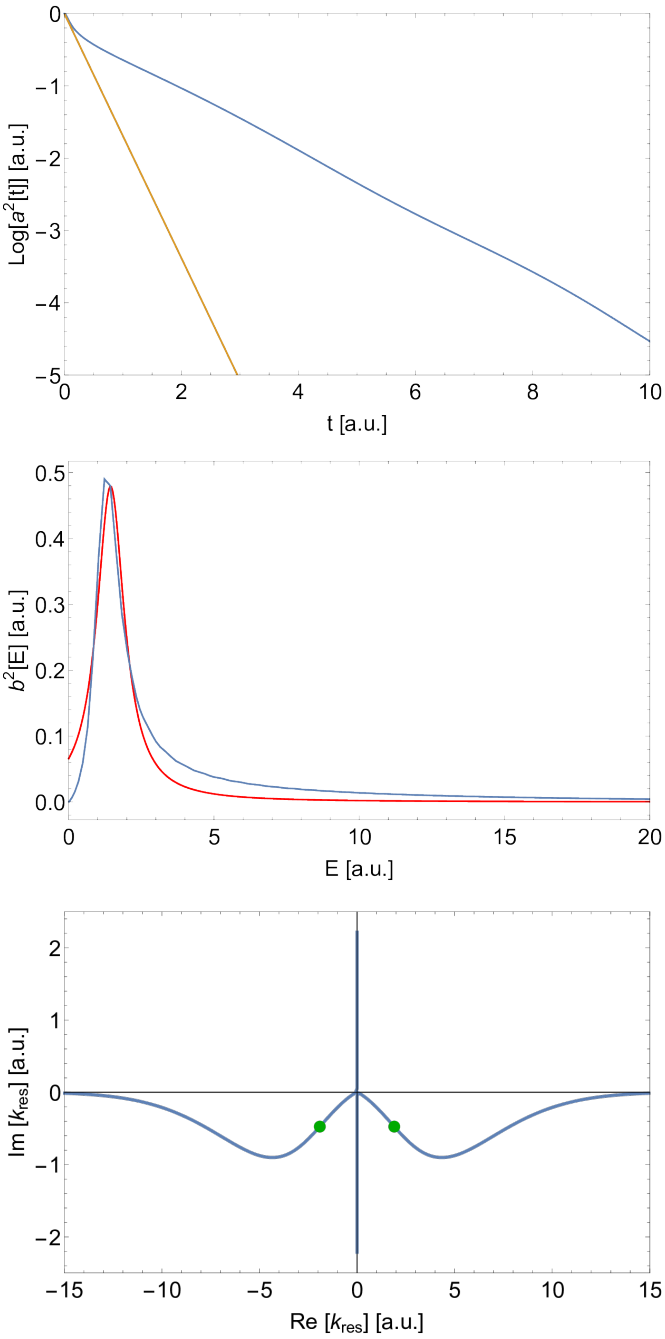

k_{res}	$Re[E_{res}]$	Γ_{res}	Γ^{1PT}	Γ_s	E_s
$\pm 1.91 - 0.48i$	1.71	1.82	3.89	1.15 ± 0.01	1.44 ± 0.1

Figure 3.9: The system is defined by coupling 3.2 with parameters $A = 20$ and $B = 20$, and by position of the discrete state $E_\varphi = 5$.
First: time evolution $|a|^2$ given by 1.51 – blue curve – and first order perturbation prediction 2.5 – yellow curve (in common logarithmic scale). Second: the spectrum $|b|^2$ given by 1.48 – blue curve – fitted with function 3.7 – red curve. Third: the position of the resonant poles (green dots). Fourth: table of parameters and poles positions. The fitted slope of the blue line on first figure is 0.93 ± 0.01.

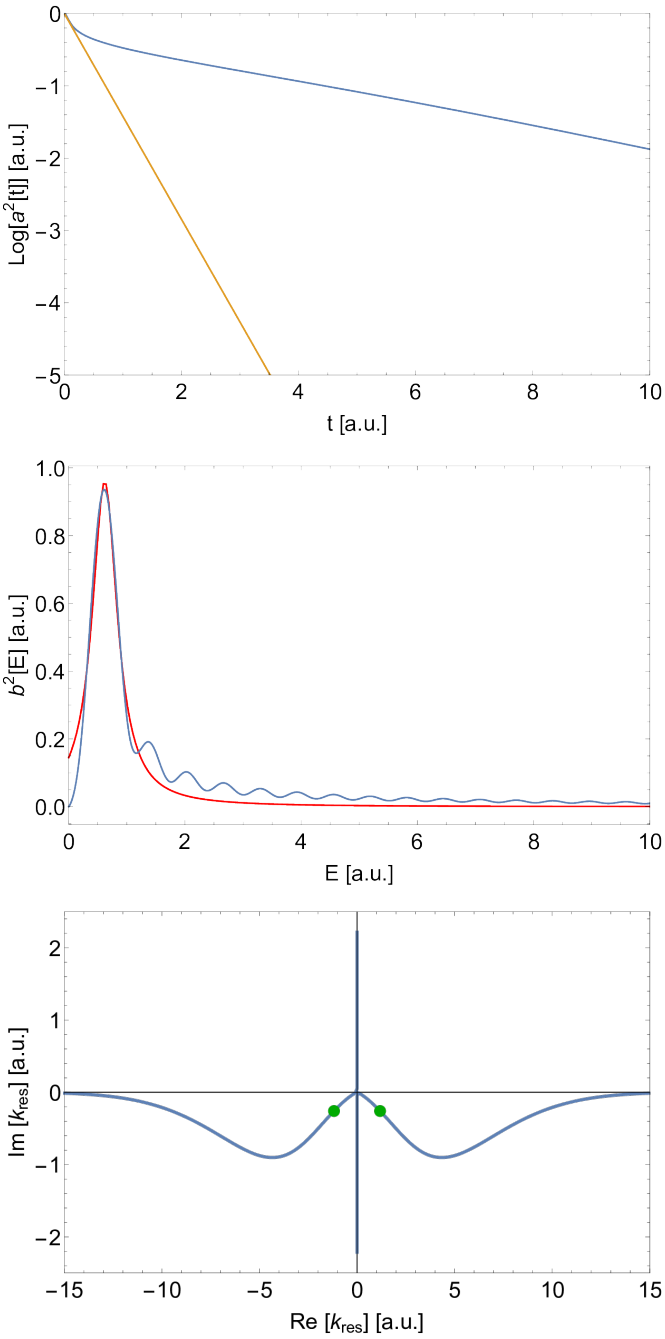

k_{res}	$Re[E_{res}]$	Γ_{res}	Γ^{1PT}	Γ_s	E_s
$\pm 1.18 - 0.26i$	0.66	0.62	3.27	0.52 ± 0.01	0.62 ± 0.01

Figure 3.10: The system is defined by coupling 3.2 with parameters $A = 20$ and $B = 20$, and by position of the discrete state $E_\varphi = 4$.
First: time evolution $|a|^2$ given by 1.51 – blue curve – and first order perturbation prediction 2.5 – yellow curve (in common logarithmic scale). Second: the spectrum $|b|^2$ given by 1.48 – blue curve – fitted with function 3.7 – red curve. Third: the position of the resonant poles (green dots). Fourth: table of parameters and poles positions. The fitted slope of the blue line on first figure is 0.35 ± 0.01.

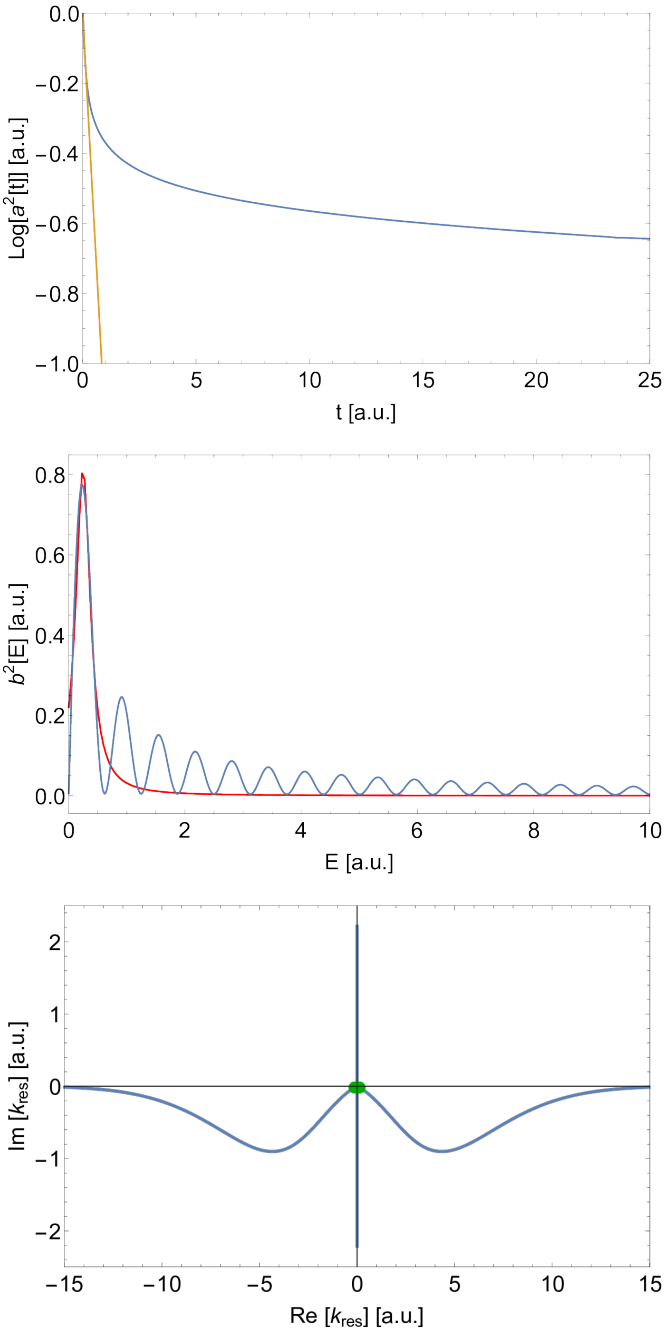

k_{res}	$Re[E_{res}]$	Γ_{res}	Γ^{1PT}	Γ_s	E_s
$\pm 0.13 - 0.02i$	0.01	0.01	2.73	0.30 ± 0.01	0.25 ± 0.01

Figure 3.11: The system is defined by coupling 3.2 with parameters $A = 20$ and $B = 20$, and by position of the discrete state $E_\varphi = 3.2$.
First: time evolution $|a|^2$ given by 1.51 – blue curve – and first order perturbation prediction 2.5 – yellow curve (in common logarithmic scale). Second: the spectrum $|b|^2$ given by 1.48 – blue curve – fitted with function 3.7 – red curve. Third: the position of the resonant poles (green dots). Fourth: table of parameters and poles positions.

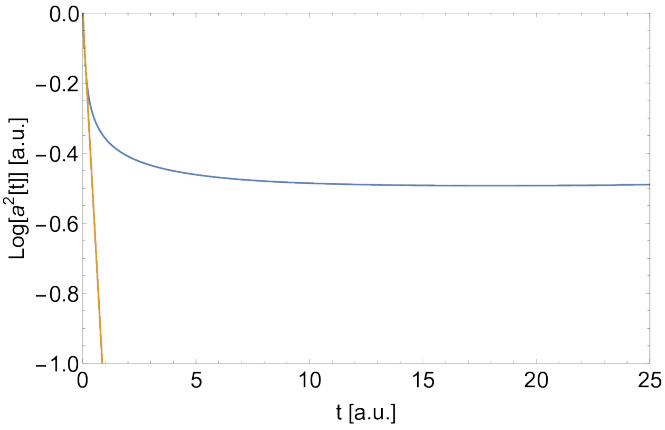

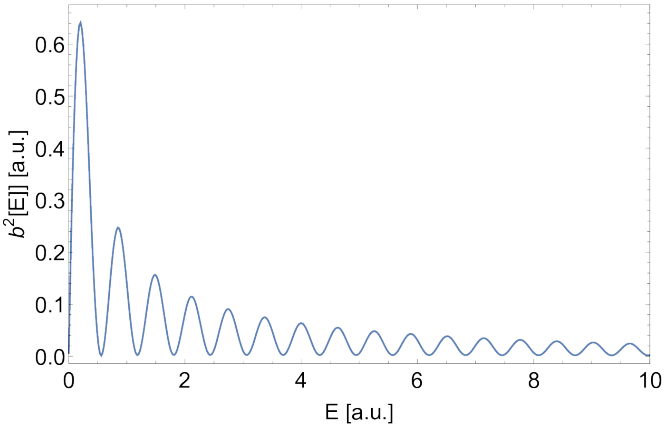

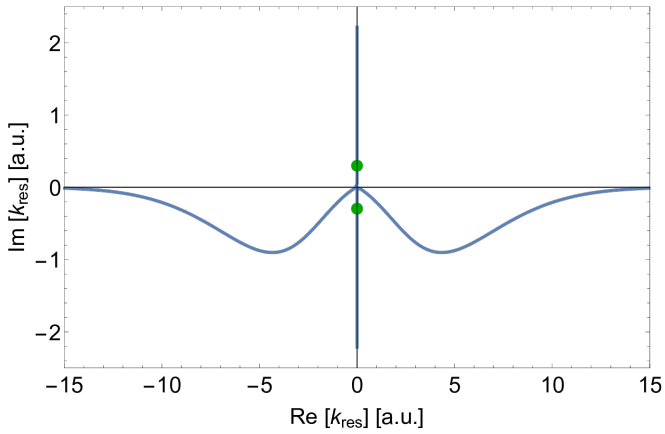

$k_{res} Im[k_{res}]$	$Re[E_{res}]$	Γ_{res}	Γ^{1PT}	Γ_s	E_s
$0 \pm 0.30i$	-0.04	0	2.65	–	–

Figure 3.12: The system is defined by coupling 3.2 with parameters $A = 20$ and $B = 20$, and by position of the discrete state $E_\varphi = 3.1$.
First: time evolution $|a|^2$ given by 1.51 – blue curve – and first order perturbation prediction 2.5 – yellow curve (in common logarithmic scale). Second: the spectrum $|b|^2$ given by 1.48 – blue curve. The function 3.7 cannot be fitted any more. Third: the position of the resonant poles (green dots). Fourth: table of parameters and poles positions.

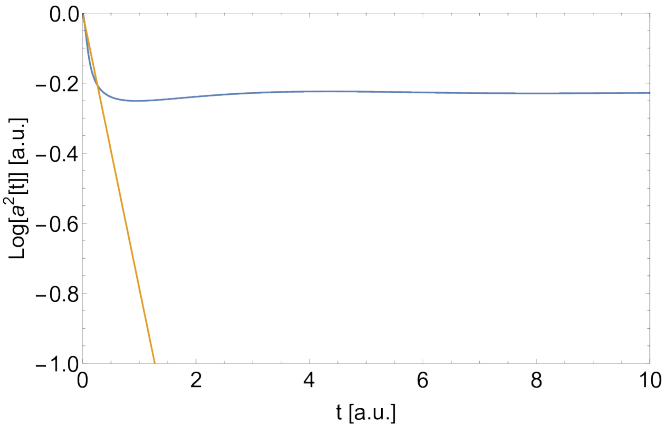

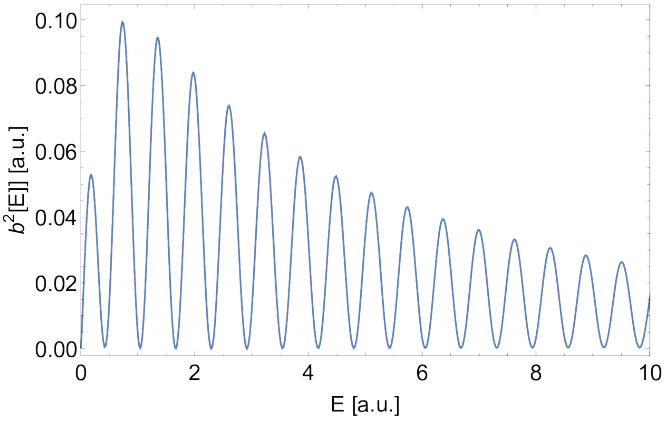

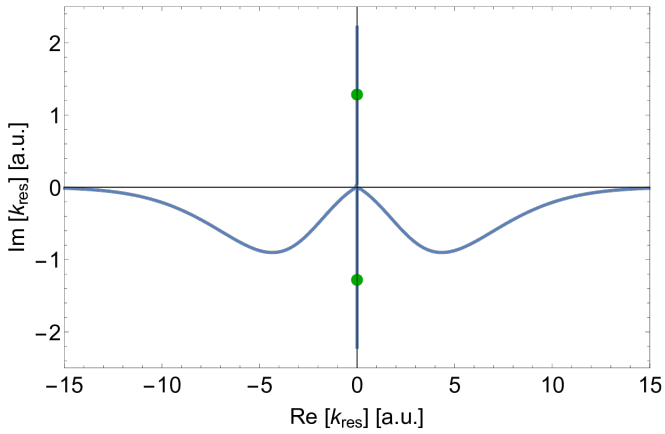

$k_{res}k_{res}$	$Re[E_{res}]$	Γ_{res}	Γ^{1PT}	Γ_s	E_s
$0 \pm 1.28i$	-0.82	0	1.81	–	–

Figure 3.13: The system is defined by coupling 3.2 with parameters $A = 20$ and $B = 20$, and by position of the discrete state $E_\varphi = 2$.
First: time evolution $|a|^2$ given by 1.51 – blue curve – and first order perturbation prediction 2.5 – yellow curve (in common logarithmic scale). Second: the spectrum $|b|^2$ given by 1.48 – blue curve. The function 3.7 cannot be fitted any more. Third: the position of the resonant poles (green dots). Fourth: table of parameters and poles positions.

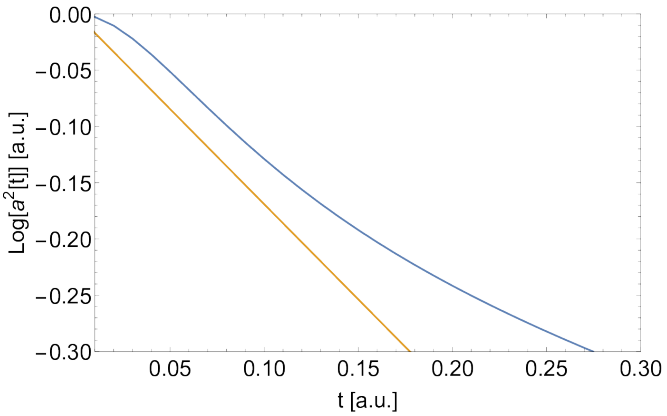

Figure 3.14: Detailed time evolution of 3.9. The system is defined by coupling 3.2 with parameters $A = 20$ and $B = 20$, and by position of the discrete state $E_\varphi = 5$.
The blue curve shows the time evolution $|a|^2$ given by 1.51 and the yellow curve shows the first order perturbation prediction 2.5, $\Gamma^{1PT} = 1.15$ (in common logarithmic scale).

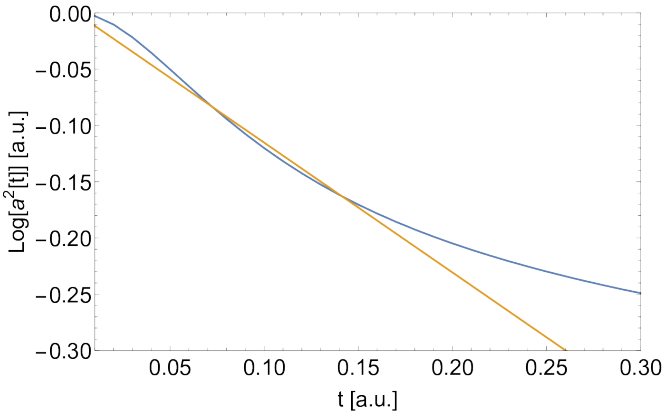

Figure 3.15: Detailed time evolution of 3.12. The system is defined by coupling 3.2 with parameters $A = 20$ and $B = 20$, and by position of the discrete state $E_\varphi = 3.1$.
The blue curve shows the time evolution $|a|^2$ given by 1.51 and the yellow curve shows the first order perturbation prediction 2.5, $\Gamma^{1PT} = 2.65$ (in common logarithmic scale).

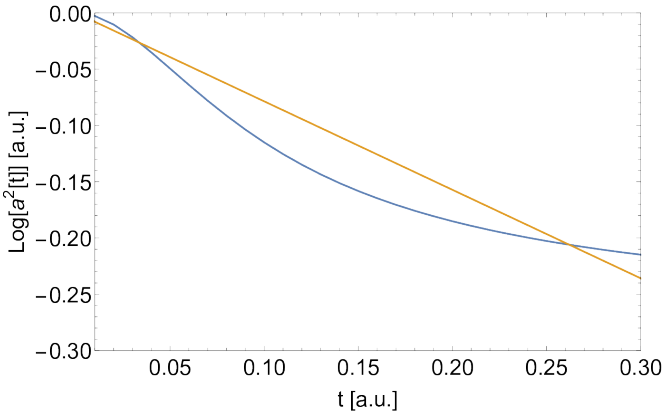

Figure 3.16: Detailed time evolution of 3.13. The system is defined by coupling 3.2 with parameters $A = 20$ and $B = 20$, and by position of the discrete state $E_\varphi = 2$.
The blue curve shows the time evolution $|a|^2$ given by 1.51 and the yellow curve shows the first order perturbation prediction 2.5, $\Gamma^{1PT} = 1.81$ (in common logarithmic scale).

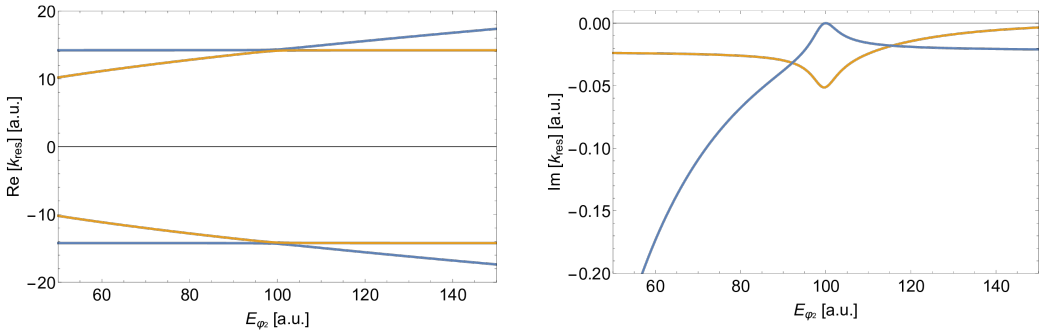

Figure 3.17: Real and imaginary part of the position of the resonant pole k_{res_1} and k_{res_2} given by 3.4 as a function of E_{φ_2}. The system is defined by $E_{\varphi_1} = 100$ and couplings 3.1, where $A_1 = 20$, $A_2 = 30$, and $B_1 = B_2 = 20$.

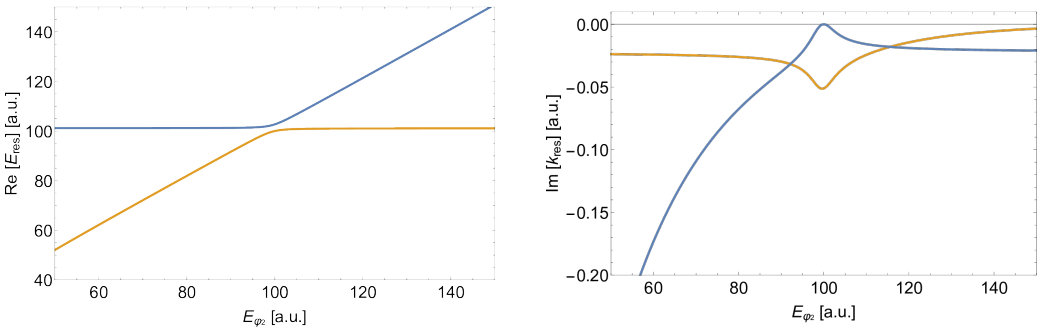

Figure 3.18: Real and imaginary part of the position of the resonant pole E_{res_1} and E_{res_2} given by 3.3 as a function of E_{φ_2}. The system is defined by $E_{\varphi_1} = 100$ and couplings 3.1, where $A_1 = 20$, $A_2 = 30$, and $B_1 = B_2 = 20$.

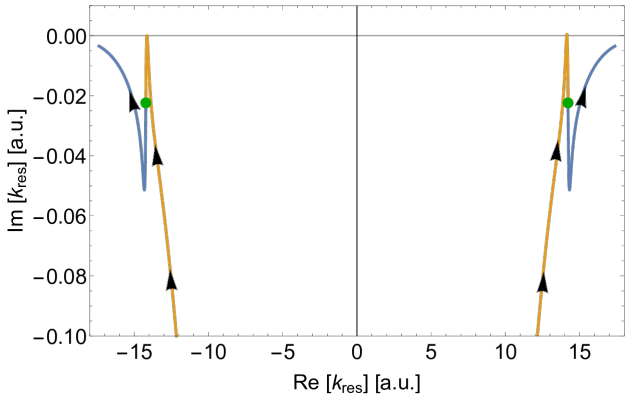

Figure 3.19: The positions of the resonant poles k_{res_1} (blue) and k_{res_2} (yellow). They are given by 3.4 as a function of E_{φ_2}. The black arrows indicate the poles moving along the curves when enlarging E_{φ_2}. The green dots are symbolising the position of the pole for only one discrete state $E_{\varphi_1} = 100$ – compare with figure 3.5. The system is defined by $E_{\varphi_1} = 100$, with couplings 3.1, where $A_1 = 20$, $A_2 = 30$, and $B_1 = B_2 = 20$.

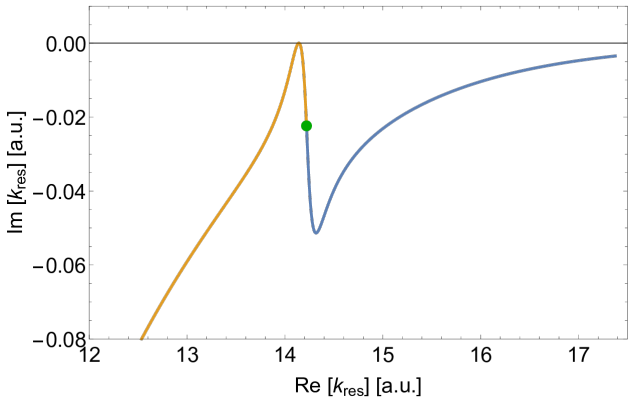

Figure 3.20: The positions of the resonant poles k_{res_1} (blue) and k_{res_2} (yellow) in detail. Only the poles with $Re[k_{res}]$ are shown for better demonstration. The positions of the poles are given by 3.4 as a function of E_{φ_2}. The green dot is symbolising the position of the pole for only one discrete state $E_{\varphi_1} = 100$ – compare with figure 3.5. The system is defined by $E_{\varphi_1} = 100$, with couplings 3.1, where $A_1 = 20$, $A_2 = 30$, and $B_1 = B_2 = 20$.

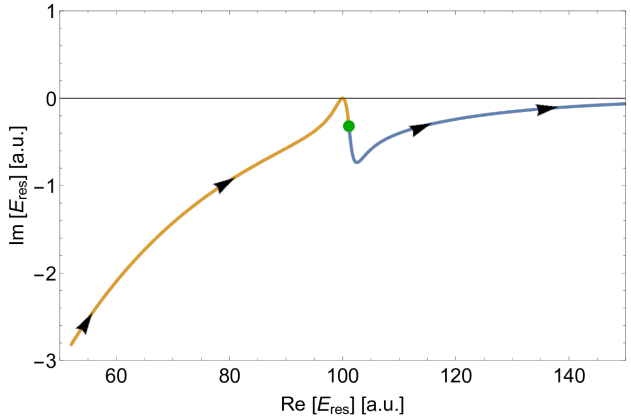

Figure 3.21: The positions of the resonant poles E_{res_1} (blue) and E_{res_2} (yellow). They are given by 3.3 as a function of E_{φ_2}. The black arrows indicate the poles moving along the curves when enlarging E_{φ_2}. The green dots are symbolising the position of the pole for only one discrete state $E_{\varphi_1} = 100$ – compare with figure 3.5. The system is defined by $E_{\varphi_1} = 100$, with couplings 3.1, where $A_1 = 20$, $A_2 = 30$, and $B_1 = B_2 = 20$.

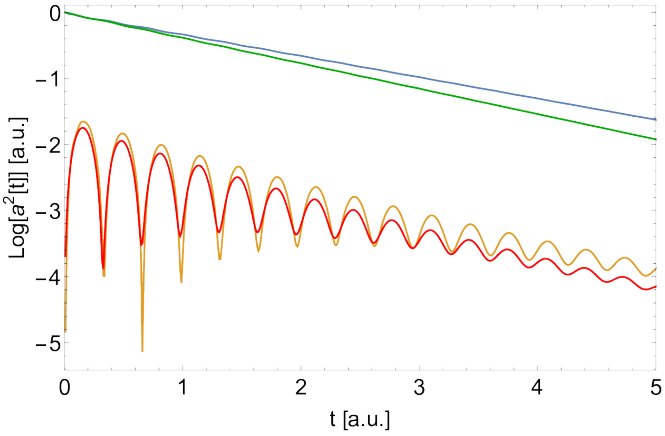

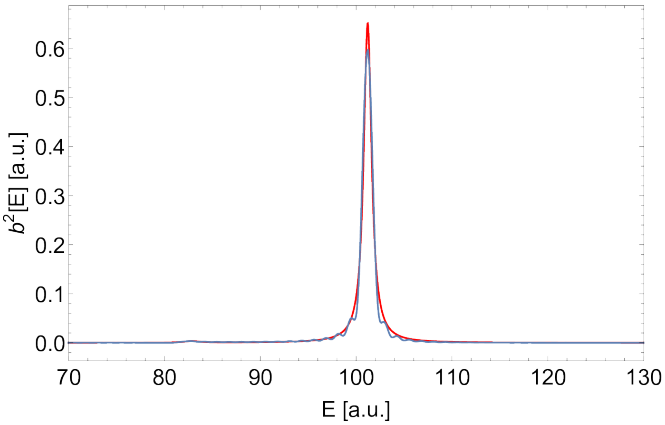

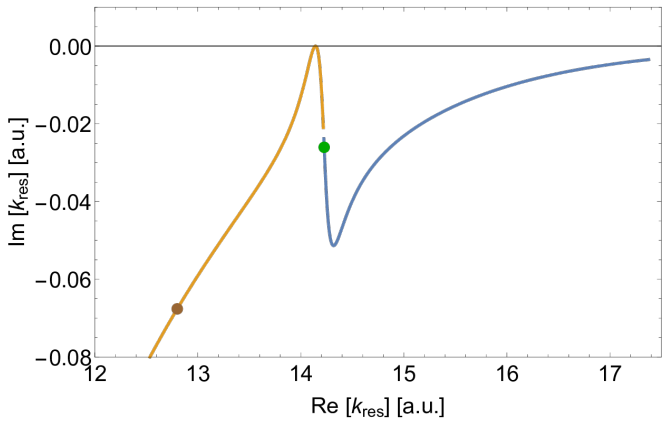

k_{res}	$Re[E_{res}]$	Γres	$Re[I_{\pm}]$	$\Gamma_{\pm}$	Γ_s	E_s
$14.22 - 0.267i$	101.19	0.74	101.23	0.88	0.99 ± 0.01	101.20 ± 0.1
$12.80 - 0.026i$	81.92	1.72	82.99	1.98	1.93 ± 1.15	82.87 ± 0.5

Figure 3.22: The system is defined by coupling 3.1 with parameters $E_{\varphi_1} = 100$, $E_{\varphi_2} = 80$, $A_1 = 20$, $A_2 = 30$, and $B_1 = B_2 = 20$.
First: time evolution of $|a_1|^2$ - blue curve – and $|a_2|^2$ – yellow curve – given by equation 2.12, the red and green curves are $e^{I_{\pm}t}$ from equation 2.24 (in common logarithmic scale). Second: the spectrum $|b|^2$ given by 1.48 – blue curve – fitted with sum of two function 3.7 – red curve. Third: the position of the resonant poles (green and brown dot), only the poles with $Re[k] > 0$ are shown for better demonstration. Fourth: table of parameters and poles positions.

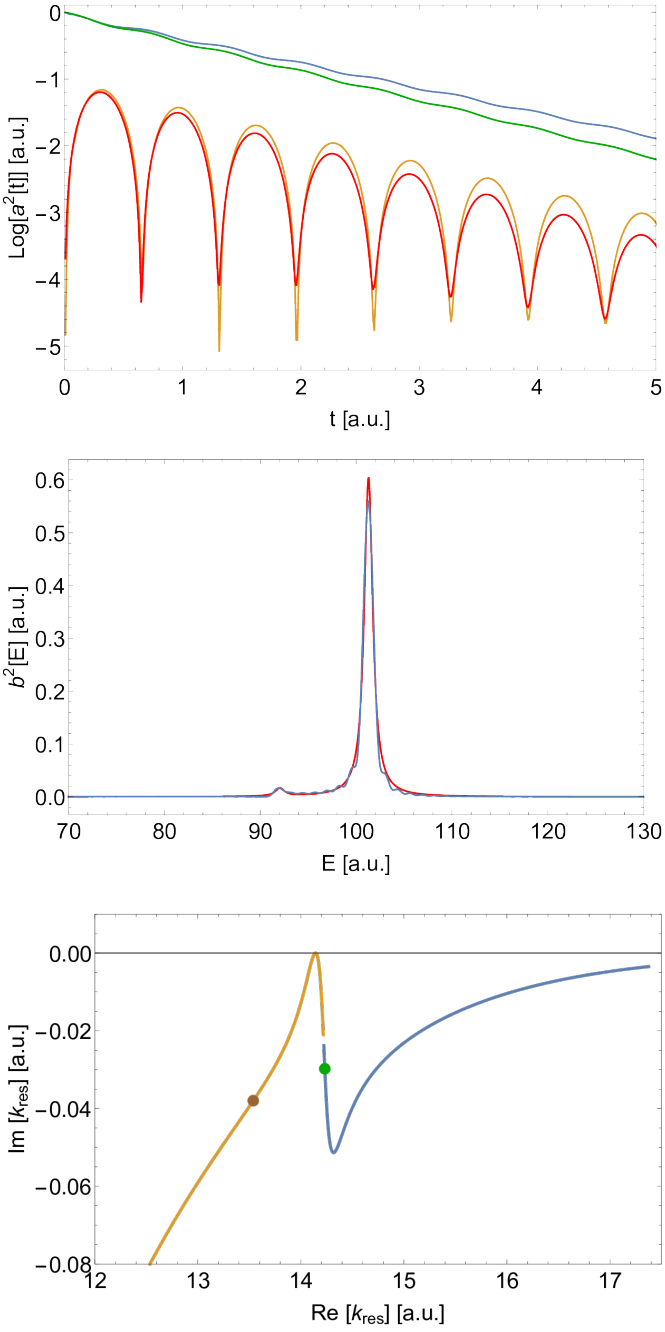

k_{res}	$Re[E_{res}]$	Γres	$Re[I_{\pm}]$	$\Gamma_{\pm}$	Γ_s	E_s
$14.23 - 0.030i$	101.28	0.84	101.32	1.00	1.06 ± 0.01	101.27 ± 0.01
$13.54 - 0.038i$	91.64	1.02	91.70	1.18	1.14 ± 0.19	92.04 ± 0.07

Figure 3.23: The system is defined by coupling 3.1 with parameters $E_{\varphi_1} = 100$, $E_{\varphi_2} = 90$, $A_1 = 20$, $A_2 = 30$, and $B_1 = B_2 = 20$.
First: time evolution of $|a_1|^2$ – blue curve – and $|a_2|^2$ – yellow curve – given by equation 2.12, the red and green curves are $e^{I_{\pm}t}$ from equation 2.24 (in common logarithmic scale). Second: the spectrum $|b|^2$ given by 1.48 – blue curve – fitted with sum of two function 3.7 – red curve. Third: the position of the resonant poles (green and brown dot), only the poles with $Re[k] > 0$ are shown for better demonstration. Fourth: table of parameters and poles positions.

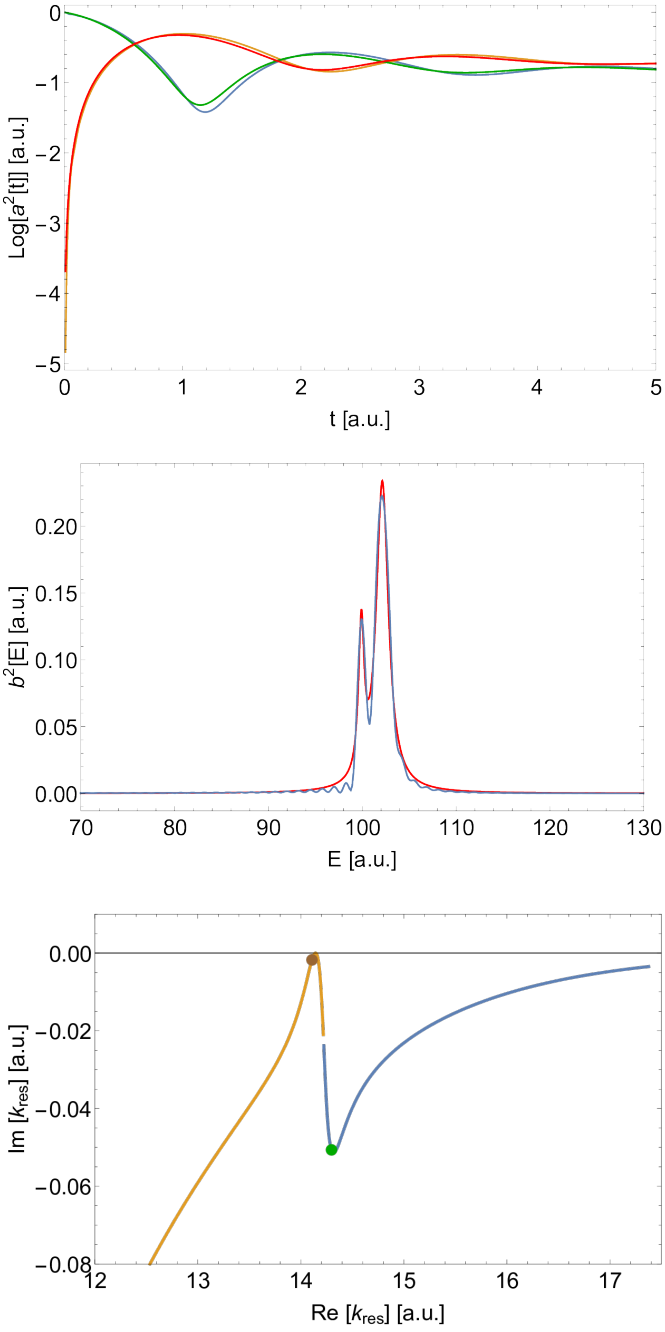

k_{res}	$Re[E_{res}]$	Γres	$Re[I_{\pm}]$	$\Gamma_{\pm}$	Γ_s	E_s
$14.30 - 0.051i$	102.21	1.44	102.31	1.64	1.56 ± 0.01	102.14 ± 0.01
$14.11 - 0.002i$	99.52	0.04	99.52	0.05	0.71 ± 0.19	99.90 ± 0.01

Figure 3.24: The system is defined by coupling 3.1 with parameters $E_{\varphi_1} = 100$, $E_{\varphi_2} = 99$, $A_1 = 20$, $A_2 = 30$, and $B_1 = B_2 = 20$.
First: time evolution of $|a_1|^2$ – blue curve – and $|a_2|^2$ – yellow curve – given by equation 2.12, the red and green curves are $e^{I_{\pm}t}$ from equation 2.24 (in common logarithmic scale). Second: the spectrum $|b|^2$ given by 1.48 – blue curve – fitted with sum of two function 3.7 – red curvee. Third: the position of the resonant poles (green and brown dot), only the poles with $Re[k] > 0$ are shown for better demonstration. Fourth: table of parameters and poles positions.

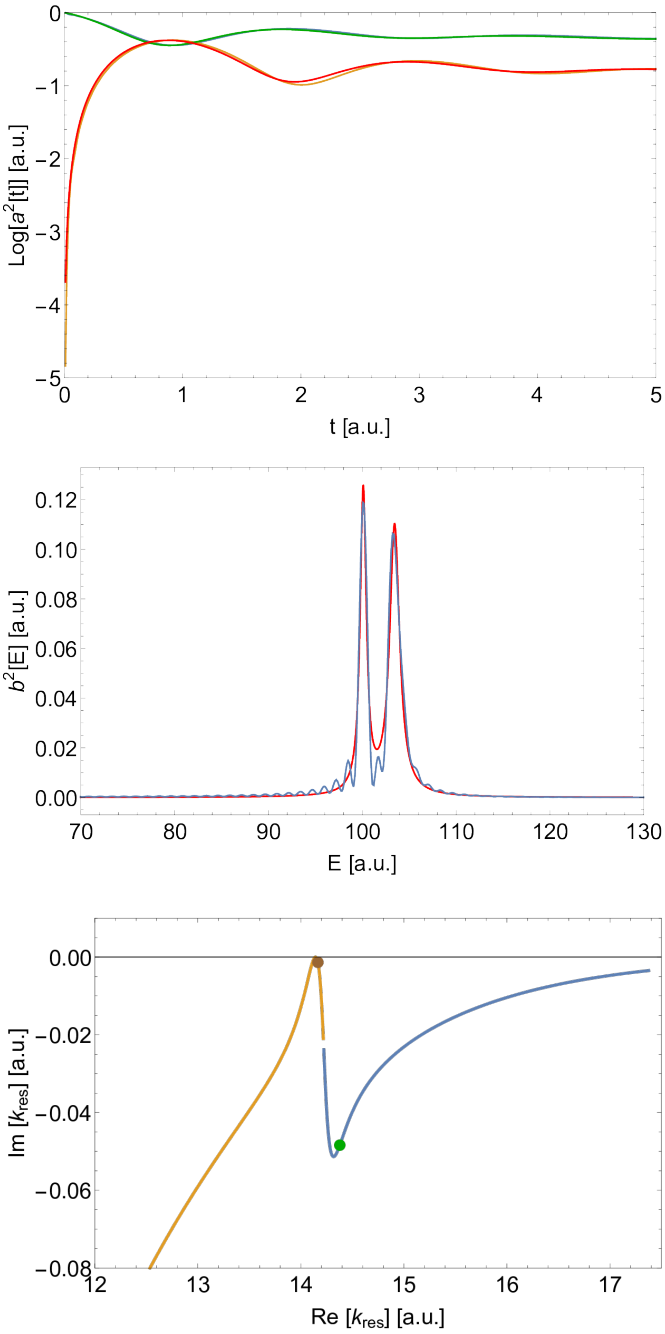

k_{res}	$Re[E_{res}]$	Γres	$Re[I_{\pm}]$	$\Gamma_{\pm}$	Γ_s	E_s
$14.37 - 0.048i$	103.36	1.39	103.58	1.51	1.28 ± 0.01	103.45 ± 0.01
$14.17 - 0.001i$	100.33	0.04	100.33	0.04	0.78 ± 0.01	100.10 ± 0.01

Figure 3.25: The system is defined by coupling 3.1 with parameters $E_{\varphi_1} = 100$, $E_{\varphi_2} = 101$, $A_1 = 20$, $A_2 = 30$, and $B_1 = B_2 = 20$.
First: time evolution of $|a_1|^2$ – blue curve – and $|a_2|^2$ - yellow curve – given by equation 2.12, the red and green curves are $e^{I_{\pm}t}$ from equation 2.24 (in common logarithmic scale). Second: the spectrum $|b|^2$ given by 1.48 – blue curve – fitted with sum of two function 3.7 – red curve. Third: the position of the resonant poles (green and brown dot), only the poles with $Re[k] > 0$ are shown for better demonstration. Fourth: table of parameters and poles positions.

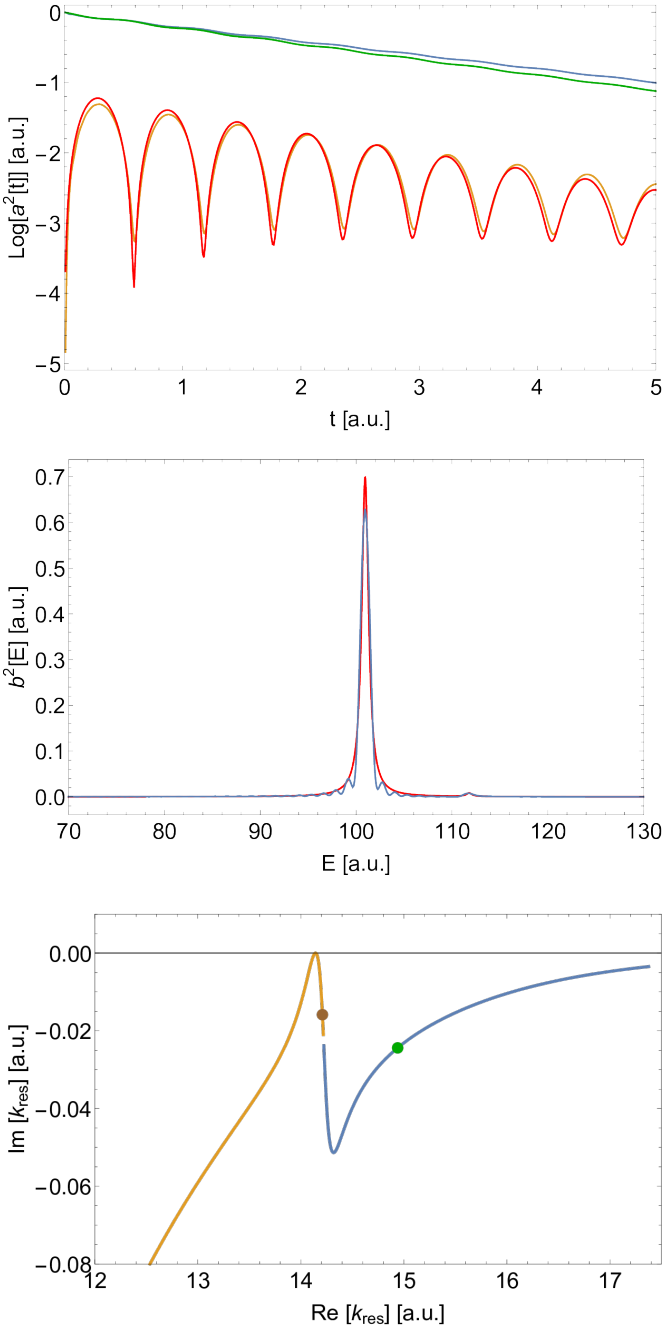

k_{res}	$Re[E_{res}]$	Γres	$Re[I_{\pm}]$	$\Gamma_{\pm}$	Γ_s	E_s
$14.94 - 0.244i$	111.60	0.72	111.65	0.84	0.85 ± 0.56	111.79 ± 0.17
$14.21 - 0.016$	100.95	0.45	100.98	0.50	0.50 ± 0.01	100.94 ± 0.01

Figure 3.26: The system is defined by coupling 3.1 with parameters $E_{\varphi_1} = 110$, $E_{\varphi_2} = 110$, $A_1 = 20$, $A_2 = 30$, and $B_1 = B_2 = 20$.
First: time evolution of $|a_1|^2$ – blue curve – and $|a_2|^2$ – yellow curve – given by equation 2.12, the red and green curves are $e^{I_{\pm}t}$ from equation 2.24 (in common logarithmic scale). Second: the spectrum $|b|^2$ given by 1.48 – blue curve – fitted with sum of two function 3.7 – red curve. Third: the position of the resonant poles (green and brown dot), only the poles with $Re[k] > 0$ are shown for better demonstration. Fourth: table of parameters and poles positions.

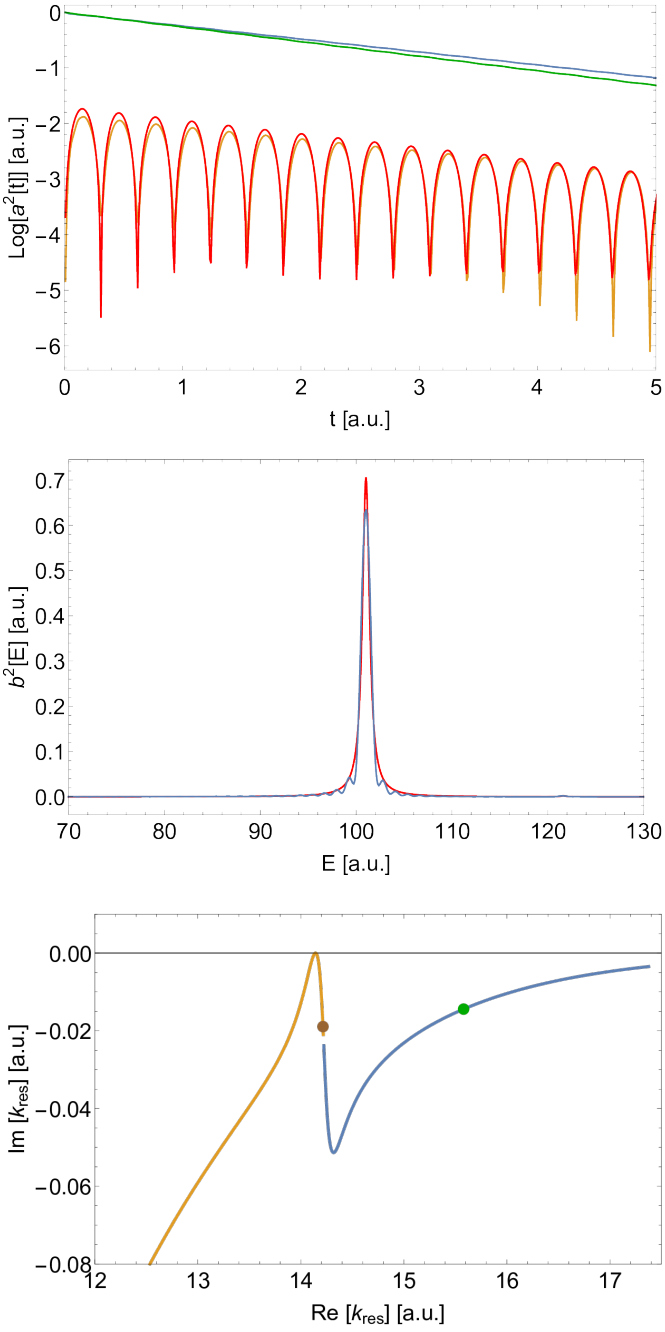

k_{res}	$Re[E_{res}]$	Γres	$Re[I_{\pm}]$	$\Gamma_{\pm}$	Γ_s	E_s
$15.58 - 0.014i$	121.36	0.22	121.40	0.52	0.55 ± 0.95	121.61 ± 0.61
$14.21 - 0.019$	101.03	0.27	101.06	0.60	0.88 ± 0.01	101.02 ± 0.01

Figure 3.27: The system is defined by coupling 3.1 with parameters $E_{\varphi_1} = 100$, $E_{\varphi_2} = 120$, $A_1 = 20$, $A_2 = 30$, and $B_1 = B_2 = 20$.
First: time evolution of $|a_1|^2$ – blue curve – and $|a_2|^2$ – yellow curve – given by equation 2.12, the red and green curves are $e^{I_{\pm}t}$ from equation 2.24 (in common logarithmic scale). Second: the spectrum $|b|^2$ given by 1.48 – blue curve – fitted with sum of two function 3.7 – red curve. Third: the position of the resonant poles (green and brown dot), only the poles with $Re[k] > 0$ are shown for better demonstration. Fourth: table of parameters and poles positions.

4. Application

In this chapter, we use the theoretical model described above for a realistic case – a neon-helium-neon cluster decaying via the interatomic Coulombic decay (ICD) [12]. The nature of ICD is as follows: Let us have a cluster with two subunits A and B. Removing one of the inner-valence electrons from the subunit B creates a ionized state. If the energy of of this state is higher than the double ionization threshold of the cluster, the process of ICD sets in. The energy excess from the subunit B^+ is used for removing outer-valence electron from the subunit A resulting in a doubly ionized cluster of the two single positive charged subunits A^+ and B^+.

We associate these two subunits with the two neon atoms in our cluster. The helium atom acts as a bridge allowing the process to be much faster compared to isolated neon dimer [13].

Our focus will be on a physical ICD process

$$\mathrm{Ne}^+(2s^{-1}) - \mathrm{He} - \mathrm{Ne} \longrightarrow \mathrm{Ne}^+(2p^{-1}) - \mathrm{He} - \mathrm{Ne}^+(2p^{-1}), \tag{4.1}$$

for such interatomic distance R that it interacts with another resonance, namely

$$\mathrm{Ne}^+(2p^{-1}) - \mathrm{He}^* - \mathrm{Ne} \longrightarrow \mathrm{Ne}^+(2p^{-1}) - \mathrm{He} - \mathrm{Ne}^+(2p^{-1}). \tag{4.2}$$

The decay of $\mathrm{Ne}^+(2s^{-1}) - \mathrm{He} - \mathrm{Ne}$ is in fact a multi-channel problem, but we restrict ourselves to a single-channel decay for simplicity.

The characteristic dependence of the ICD width on the interatomic neon – neon distance R is

$$\Gamma(R) \propto \frac{1}{R^6}, \tag{4.3}$$

corresponding to dipole–dipole interaction between the two subunits [14, 15]. For Ref. [13] the energy dependent decay widths $\Gamma(E,R) = 2\pi|V(E,R)|^2$ of the two aforementioned resonances were computed using *ab initio* Fano-ADC method [16]. In order to apply the same techniques as in the previous chapter, we fit the *ab initio* data by a slightly generalized formula for the discrete state – continuum coupling

$$V_i(E) = \begin{cases} \sqrt{\frac{A_i}{2\pi}\left(\frac{E}{B_i}\right)^{\alpha_i}\exp\left(-\frac{E}{B_i}\right)} & E > 0 \\ 0 & E < 0 \end{cases}, \tag{4.4}$$

with

$$A_i = \frac{A_{0i}}{R_i^6}, \tag{4.5}$$

where A_{0i}, B_i, and α_i are parameters.

We shall keep the energy of one of the discrete states (which is associated with $\mathrm{Ne}^+(2s^{-1}) - \mathrm{He} - \mathrm{Ne}$) constant, $E_{\varphi_1} = 0.13632$, and parametrize the other one (associated with $\mathrm{Ne}^+(2p^{-1}) - \mathrm{He}^* - \mathrm{Ne}$)

$$E_{\varphi_2} = \frac{d}{R^e} + f. \tag{4.6}$$

The fitted parameters are in table 4.1.

A_{01}	5.7996
A_{02}	33.5139
B_1	1.1377
B_2	0.2200
α_1	0.3878
α_2	0.8407
d	2.0613
e	0.1444
f	-1.6035

Table 4.1: Fitted parameters of functions 4.4 and 4.6.

Of our main interest is the time evolution of the system for R such that we are near crossing, the spectra, and the poles of the $\mathbb{S}$-matrix operator trajectories in the complex plane.

The generalized coupling 4.4 gives rise to a different level shift function 2.2

$$F_{ij}(k) = -\frac{A_{ij}}{2\pi}\Gamma(1+\alpha_{ij})\frac{-k^2}{2B_{ij}}\Gamma\left(-\alpha_{ij}, -\frac{k^2}{2B_{ij}}\right)\exp\left(-\frac{k^2}{2B_{ij}}\right), \tag{4.7}$$

$$\alpha_{ij} = \frac{\alpha_i + \alpha_j}{2}, \tag{4.8}$$

$$B_{ij} = 2\frac{B_i B_j}{B_i + B_j}, \tag{4.9}$$

$$A_{ij} = \sqrt{\frac{A_i A_j}{B_i^{\alpha_i} B_i^{\alpha_j}}} B^{\alpha_{ij}}. \tag{4.10}$$

With this analytical form, we can start the search for the poles positions.

The real and imaginary parts of the poles position as functions of the length of the trimer $R \in (2.7, 4.2)$ are in figures 4.1 and 4.2 for k- and E-representation respectively. We can see the crossing at $R = 3.235$ A where the imaginary part of one of the poles suddenly increases while the imaginary part of the other one decreases as described in the section 3.2. In figure 4.2, we can also see the pole trajectory for only one isolated resonance associated with 4.1. The influence of the second resonance 4.2 leading to the stabilization is clearly visible – if the first resonance 4.1 is isolated, it has for $R = 3.235$ decay width $\Gamma(E_{res}) = 7.57 \times 10^{-3}$ while the same resonance interacting with the second resonance has $\Gamma(E_{res}) = 0.06 \times 10^{-3}$, which is almost a bound state in continuum as already discussed. The stabilization then leads to prolongation of the lifetime by three orders of magnitude.

The poles trajectories in momentum or energy complex plane are in figures 4.3 (k-representation) and 4.4 (E-representation). The black arrows show how the poles move along the curves with increasing R. The blue curve is associated with $E_{\varphi_1} = 0.13632$ and the yellow curve corresponds to E_{φ_1} as defined in 4.6. The influence of this crossing resonance on the constant one is well visible in following figures 4.5 to 4.9.

The time evolutions shown in figures 4.5 to 4.9 for $R = 3 - 3.4$ are calculated partly by the full simulation 2.12 (figure 4.5) and partly by adiabatic elimination

(figures 4.8 and 4.9) for such set-ups where the correction 2.18 is negligible, that is, for Γ small enough (the term 2.18 is proportional to Γ). To demonstrate that we can use the adiabatic elimination of the continuum, there are time evolutions obtained by both approaches on figures 4.6 and 4.7.

The time evolution is (apart from few oscillations at the beginning) purely exponential and after some time, the decay of both of the discrete states relaxes to decay equivalent into the slowly decaying resonance.

The spectra of systems are purely Lorentzian with the parameters Γ_s and E_s similar to the slowly decaying resonance. The spectrum of the system on crossing ($R = 3.235$A, see figure 4.7) is not perfectly converged for numerical reasons and therefore does not offer a good estimate of Γ.

Note that all Γ obtained by different approaches for each investigated R are in good agreement (except for Γ_s on crossing caused by the fact that the spectrum is not converged). The stabilization effect of this system as discussed in the previous chapter can be then observed from any of these Γ.

In the real case of a multiple-channel scattering, the stabilization effect is not that significant as the one observed here. This is because the stabilization only affects the partial decay width that corresponds to the continuum that is shared by both of the resonant states.

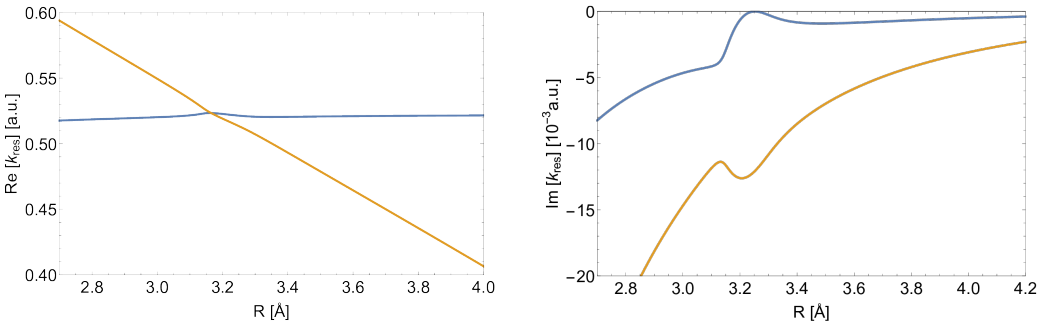

Figure 4.1: Real and imaginary part of the positions of the resonant poles k_{res_1} and k_{res_2} given by 3.4 as a function of R. The system is defined by coupling 4.4 with parameters from table 4.1, and with $E_{\varphi_1} = 0.1363$ and E_{φ_2} given by 4.6. The blue curve is associated with E_{φ_1} and the yellow curve corresponds to E_{φ_2}. Only poles with $Im[k_{res}] > 0$ are shown.

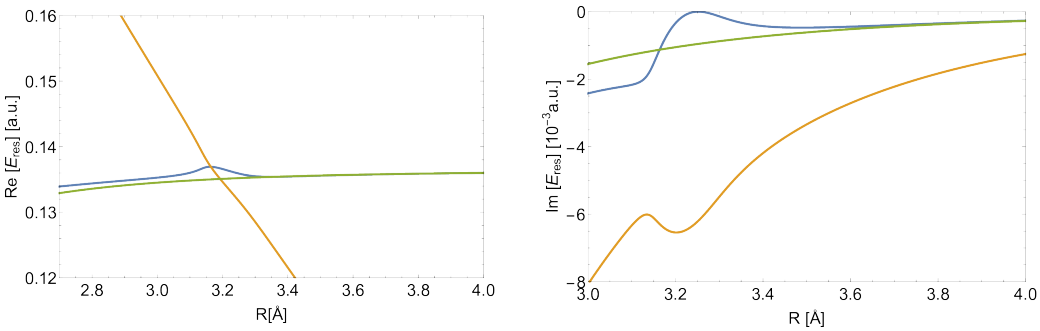

Figure 4.2: Real and imaginary part of the positions of the resonant poles E_{res_1} and E_{res_2} given by 3.3 as a function of R (blue and yellow curve). The system is defined by coupling 4.4 with parameters from table 4.1, and with $E_{\varphi_1} = 0.1363$ and E_{φ_2} given by 4.6. The blue curve is associated with E_{φ_1} and the yellow curve corresponds to E_{φ_2}. The green curve shows the pole trajectory of a system with the same parameters but with only one resonance associated with 4.1.

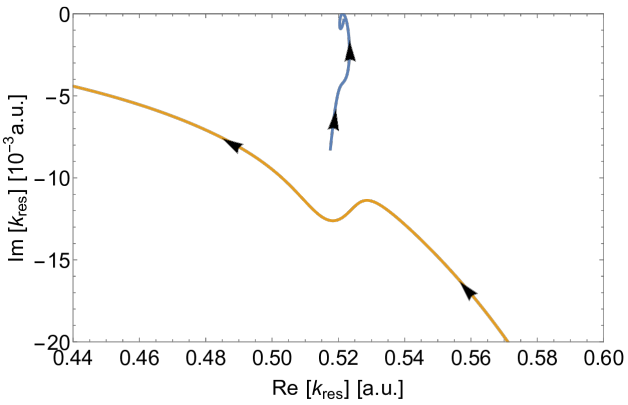

Figure 4.3: The position of the resonant poles k_{res_1} and k_{res_2} given by 3.4 as a function of R. The black arrows indicate the poles moving along the curves when enlarging R. The system is defined by coupling 4.4 with parameters from table 4.1, and with $E_{\varphi_1} = 0.1363$ and E_{φ_2} given by 4.6. The blue curve is associated with E_{φ_1} and the yellow curve corresponds to E_{φ_2}.

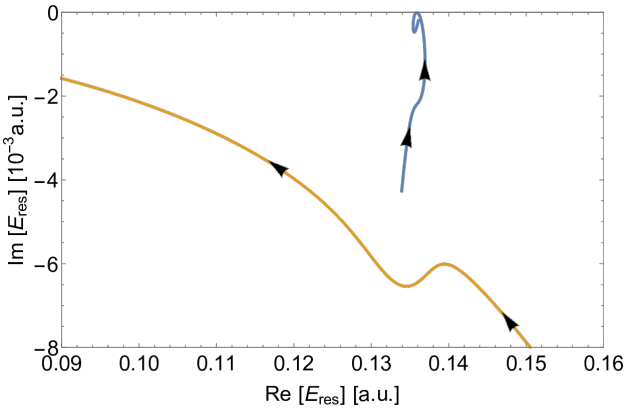

Figure 4.4: The position of the resonant poles E_{res_1} and E_{res_2} given by 3.3 as a function of R. The black arrows indicate the poles moving along the curves when enlarging R. The system is defined by coupling 4.4 with parameters from table 4.1, and with $E_{\varphi_1} = 0.1363$ and E_{φ_2} given by 4.6 The blue curve is associated with E_{φ_1} and the yellow curve corresponds to E_{φ_2}.

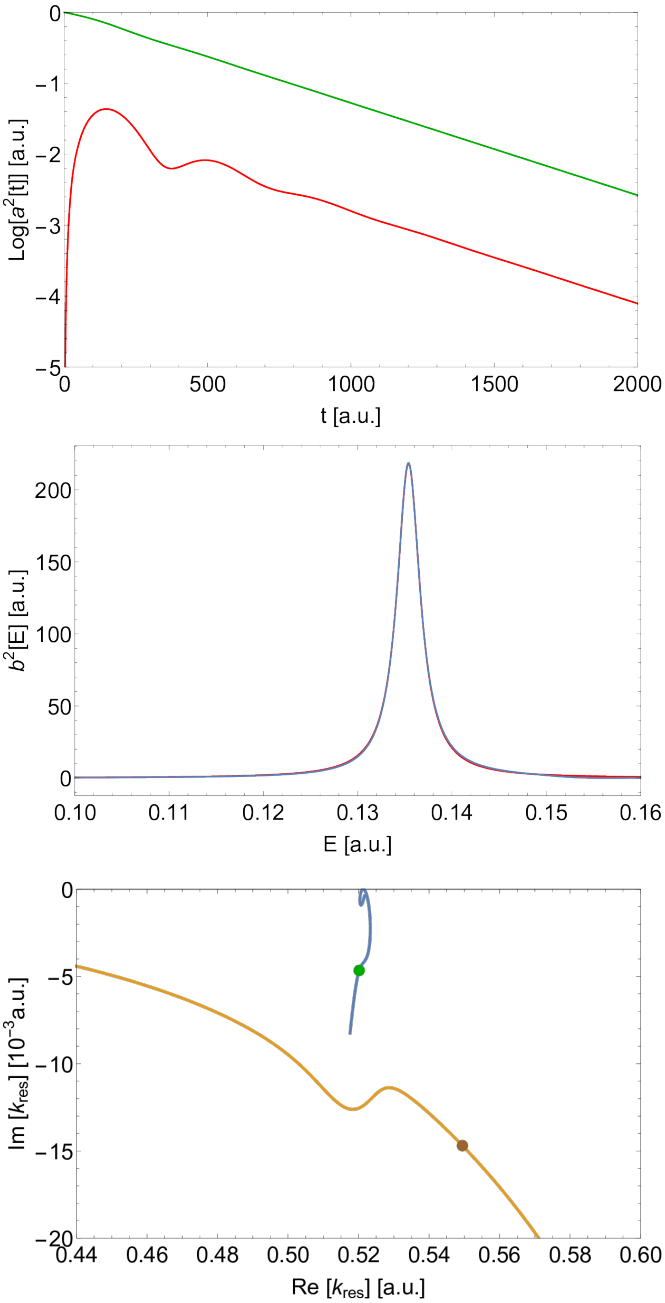

k_{res}	$\pm 0.520 - 4.65 \times 10^{-3}$	$\pm 0.549 - 14.69 \times 10^{-3}$
$Re[E_{res}]$	0.135	0.151
$\Gamma res \times 10^{-3}$	4.84	16.14
$\Gamma_s \times 10^{-3}$	4.99 ± 0.01	-
E_s	0.135 ± 0.001	-

Figure 4.5: The system is defined by coupling 4.4 with parameters given by 4.1 and $R = 3\,\mathrm{A}$, and by position of the discrete states $E_{\varphi_1} = 0.1363$ and $E_{\varphi_2} = 0.1471$ given by 4.6.
First: time evolution of $|a_1|^2$ – green curve – associated with 4.1 and $|a_2|^2$ – red curve – associated with 4.2 given by solution of 2.12 (in common logarithmic scale). Second: the spectrum $|b|^2$ given by 1.48 – blue curve – fitted with function 3.7 – red curve. Third: the position of the resonant poles (green and brown dot), only the poles with $Re[k] > 0$ are shown for better demonstration. Fourth: table of parameters and poles positions.

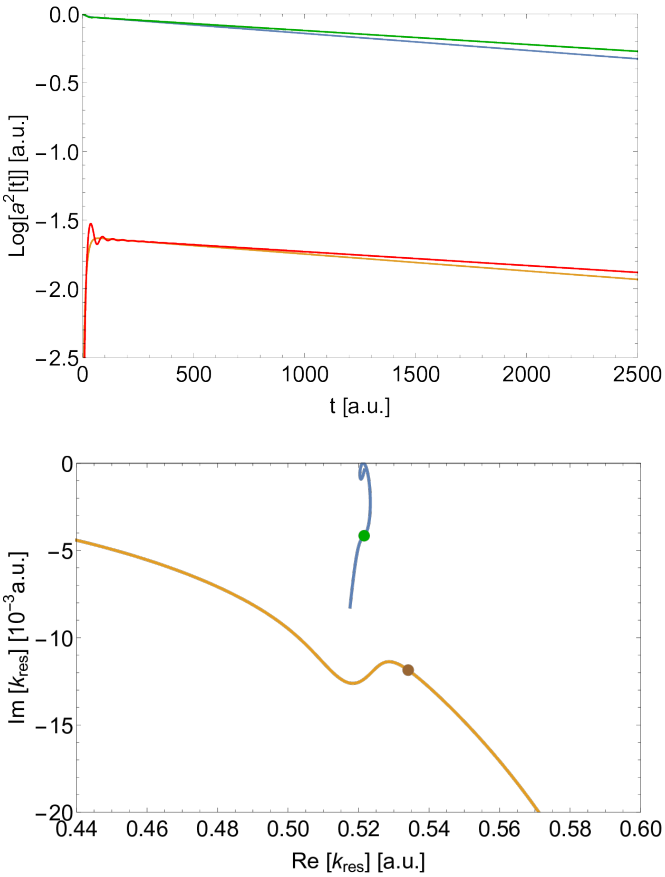

k_{res}	$\pm 0.521 - 4.15 \times 10^{-3}$	$\pm 0.534 - 11.85 \times 10^{-3}$
$Re[E_{res}]$	0.136	0.142
$\Gamma res \times 10^{-3}$	4.33	12.66
$Re[I_{\pm}]$	0.136	0.148
$\Gamma_{\pm} \times 10^{-3}$	0.28	14.02

Figure 4.6: The system is defined by coupling 4.4 with parameters given by 4.1 and $R = 3.1\,\text{Å}$, and by position of the discrete states $E_{\varphi_1} = 0.1363$ and $E_{\varphi_2} = 0.1471$ given by 4.6.
First: time evolution of $|a_1|^2$ – blue curve – and $|a_2|^2$ – yellow curve – given by solution of adiabatic elimination 2.23. The red and green curves are given by solution 2.12. (in common logarithmic scale). Second: the position of the resonant poles (green and brown dot), only the poles with $Re[k] > 0$ are shown for better demonstration. Third: table of parameters and poles positions.

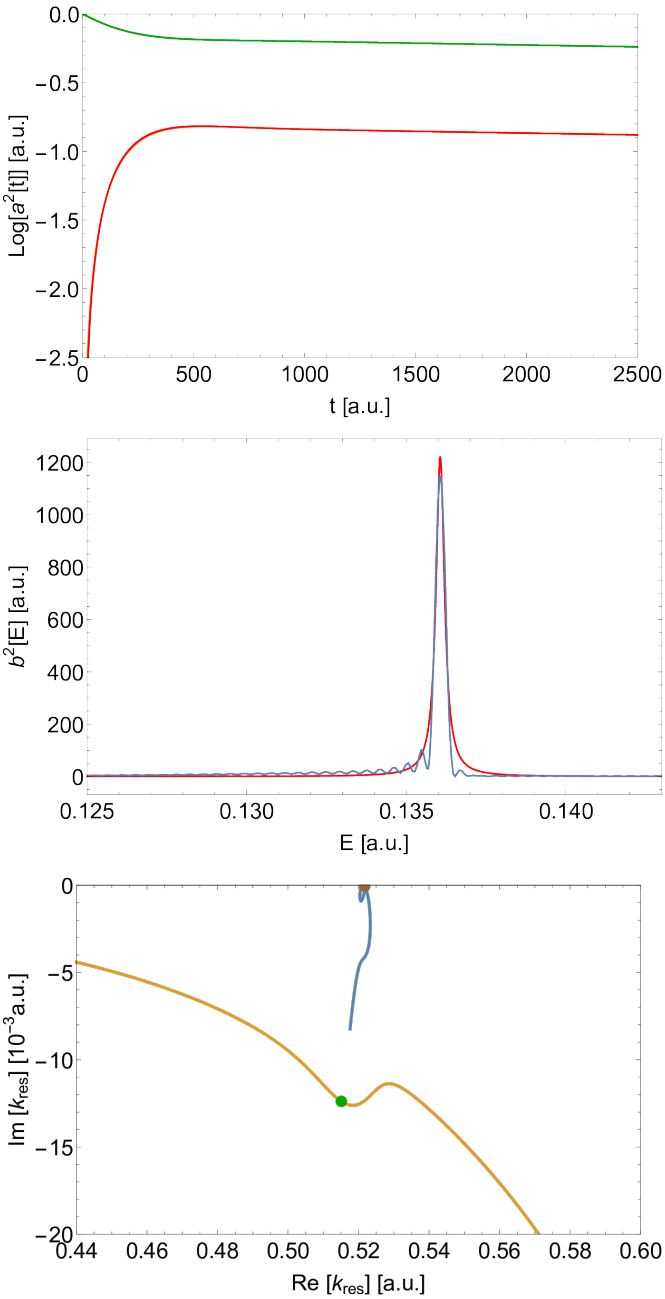

k_{res}	$\pm 0.515 - 12.38 \times 10^{-3}$	$\pm 0.521 - 0.06 \times 10^{-3}$
$Re[E_{res}]$	0.136	0.132
$\Gamma res \times 10^{-3}$	0.06	12.76
$Re[I_{\pm}]$	0.136	0.132
$\Gamma_{\pm} \times 10^{-3}$	0.06	12.43
$\Gamma_s \times 10^{-3}$	0.31 ± 0.01	
E_s	0.136 ± 0.001	

Figure 4.7: The system is defined by coupling 4.4 with parameters given by 4.1 and $R = 3.235\,\mathrm{A}$, and by position of the discrete states $E_{\varphi_1} = 0.1363$ and $E_{\varphi_2} = 0.1364$ given by 4.6.
First: time evolution of $|a_1|^2$ – blue curve – and $|a_2|^2$ – yellow curve – given by solution of adiabatic elimination 2.23. The red and green curves are given by solution 2.12. Second: the spectrum $|b|^2$ given by 1.48 – blue curve – fitted with function 3.7 – red curve. Third: the position of the resonant poles (green and brown dot), only the poles with $Re[k] > 0$ are shown for better demonstration. Fourth: table of parameters and poles positions.

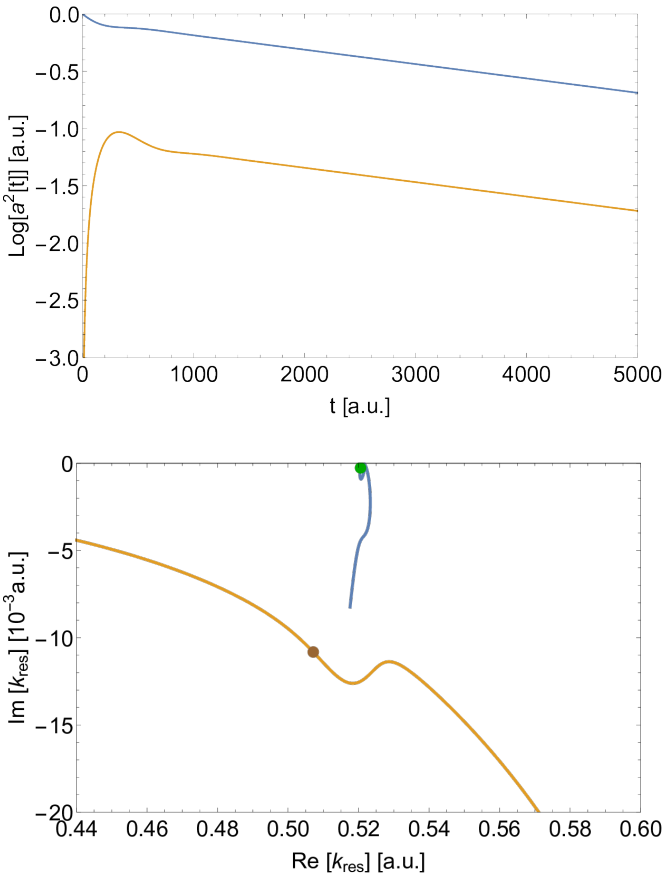

k_{res}	$\pm 0.520 - 0.27 \times 10^{-3}$	$\pm 0.507 - 10.82 \times 10^{-3}$
$Re[E_{res}]$	0.135	0.128
$\Gamma res \times 10^{-3}$	0.27	10.99
$Re[I_{\pm}]$	0.135	0.128
$\Gamma_{\pm} \times 10^{-3}$	0.29	10.71

Figure 4.8: The system is defined by coupling 4.4 with parameters given by 4.1 and $R = 3.3\,\text{Å}$, and by position of the discrete states $E_{\varphi_1} = 0.1363$ and $E_{\varphi_2} = 0.1314$ given by 4.6.
First: time evolution of $|a_1|^2$ – blue curve – associated with 4.1 and $|a_2|^2$ – yellow curve – associated with 4.2 given by solution of adiabatic elimination 2.23 (in common logarithmic scale). Second: the position of the resonant poles (green and brown dot), only the poles with $Re[k] > 0$ are shown for better demonstration. Third: table of parameters and poles positions.

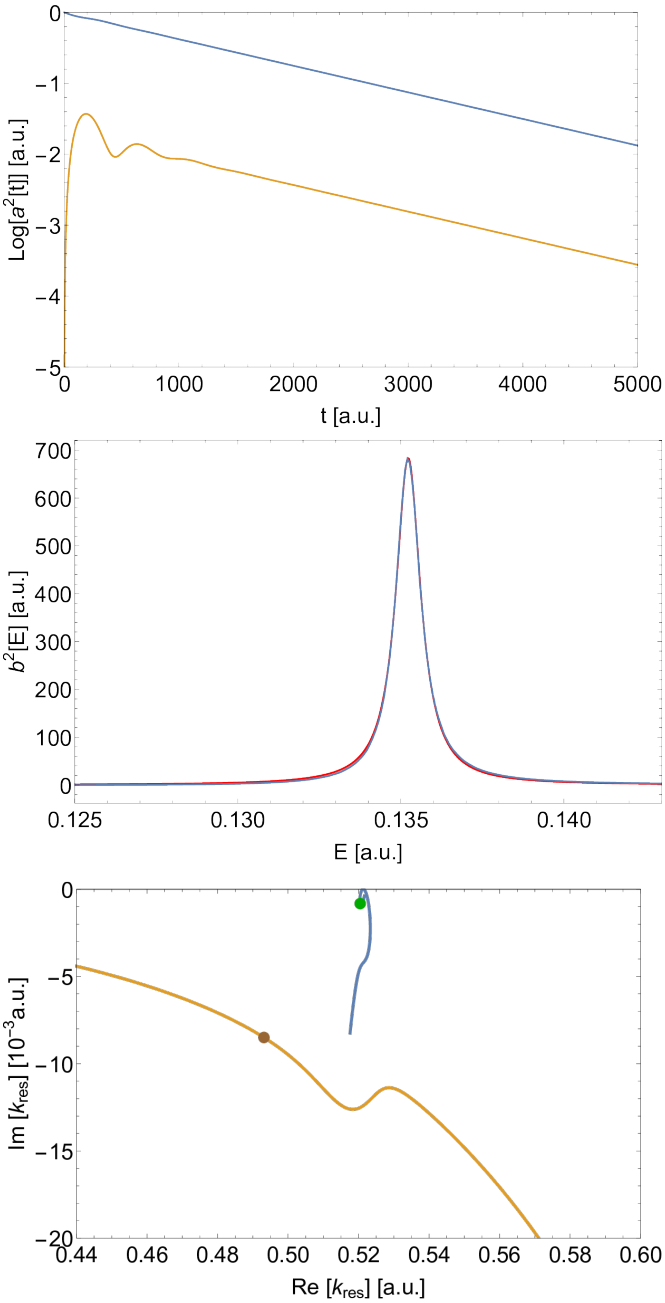

k_{res}	$\pm 0.520 - 0.82 \times 10^{-3}$	$\pm 0.493 - 8.45 \times 10^{-3}$
$Re[E_{res}]$	0.124	0.135
$\Gamma res \times 10^{-3}$	0.85	8.38
$Re[I_{\pm}]$	0.122	0.135
$\Gamma_{\pm} \times 10^{-3}$	0.86	8.22
$\Gamma_s \times 10^{-3}$	0.92 ± 0.01	-
E_s	0.135 ± 0.001	-

Figure 4.9: The system is defined by coupling 4.4 with parameters given by 4.1 and $R = 3.4\,\mathrm{A}$, and by position of the discrete states $E_{\varphi_1} = 0.1363$ and $E_{\varphi_2} = 0.1239$ given by 4.6.
First: time evolution of $|a_1|^2$ – blue curve – and $|a_2|^2$ – yellow curve – given by solution of adiabatic elimination 2.23 (in common logarithmic scale). Second: the spectrum $|b|^2$ given by 1.48 – blue curve – fitted with function 3.7 – red curve. Third: the position of the resonant poles (green and brown dot), only the poles with $Re[k] > 0$ are shown for better demonstration. Fourth: table of parameters and poles positions.

Conclusion

We now try to summarize the results obtained in this thesis. From the beginning we worked with a theoretical model of one or two metastable state(s) embedded in a continuum into which it decays. We used a suitable coupling, that is, a coupling that is analytical, continuous almost everywhere and for certain parameters leads to a bound state. For such coupling we studied the time evolution and spectra of the the system with different parameters that characterize it. We also focused on the positions of the poles of the scattering matrix and their trajectories in the complex energy or momentum plane as a function of one of the parameters of the system.

For the case of one metastable state in the system, the time evolution far above the threshold is well-approximated by first order perturbation theory up to a point, where the decay starts to be polynomial. This transition takes place earlier when pushing the metastable state closer to the threshold. When the energy of the metastable state is less than a certain critical value, the metastable state does not decay completely any more (a bound state appears).

The spectral line, close to the Lorentzian line shape in the area far above the threshold, is deformed eventually with closer threshold, turning into oscillations for the bound state.

With two metastable states in the system, we have studied the influence of the overlap on the time evolution in the area, where the threshold plays no role. We compared it with the approximation of adiabatic elimination of the continuum that gave very good results even for fairly close states. We also commented on an "avoided crossing" phenomenon observed on the poles trajectories in the complex plain.

The resonance crossing led to a stabilization of one of the resonances, that is, the decay width of one of the resonances suddenly decreased, while the other one acquires far larger decay width. This stabilization was so strong that the resonance almost did not decay any more, creating a state known as a bound state in continuum.

The last part is an application on a real system – the neon-helium-neon trimer. We have studied time evolution and spectrum of this system near the resonance crossing. The stabilization effect caused by the presence of the second resonance for a single-channel scattering approximation leads to a decrease of the decay width by three orders of magnitude. The decrease is still well described by the decay widths obtained by different approaches, namely from adiabatic elimination of the continuum, from spectra and from exact calculation of the position of the resonance pole.

For the purpose of this thesis, we used simplified single-channel scattering approach. The real case is much more complicated and leads to smaller stabilization effect. This thesis offers an upper estimate of this effect.

Bibliography

[1] J. R. Taylor. *Scattering Theory*. John Wiley and Sons, Malabar, 1972.

[2] B. H. Bransen and C. J. Joachin. *Physics of Atoms and Molecules*. second edition. Prentice Hall, Harlow, 2010.

[3] C. Cohen Tanoudji, J. Dupon Roc, and G. Grinberg. *Atom-Photon Interactions: Basic Process and Applications*. Wiley-Interscience publication. J. Wiley, University of Michigan, 1992.

[4] L. Fonda, G. C. Ghirardi, and A. Rimini. Decay theory of unstable quantum systems. *Reports on Progress in Physics*, 41:587–631, 1978.

[5] V. G. Yarzhemsky and F. P. Larkins. The shapes of Auger decay lines in photoelectron satellite spectra. *The European Physical Journal D*, 5:179–184, 1999.

[6] W. Domcke. Theory of resonance and threshold effects in electron-molecule collisions. *Physics Reports*, 208(2):97–188, 1991.

[7] M. Eckstein, N. Mayer, C. Yang, G. Sansone, M. J. J. Vrakking, M. Ivanov, and O. Kornilov. Interference stabilization of autoionizing states in molecular n2 studied by time- and angular-resolved photoelectron spectroscopy. *Faraday Discussions*, 194:509–524, 2016.

[8] M. E. Sukharev, E. Charron, A. Suzor Weiner, and M. V. Fedorov. Calculations of photodissiciation in intense laser fields: Validity of the adiabatic elimination of the continuum. *Internation Journal of Quantum Chemistry*, 99:452–459, 2004.

[9] M. V. Fedorov. Bound states in the continuum. *Journal of Physics B: Atomic and Molecular Physics*, 10(13):2572–2582, 1997.

[10] H. Gedeonová. *Time-dependent solution of the generalized Fano model, Bachelor thesis*. MFF UK, 2017.

[11] C. W. Hsu, B. Zhen, A. D. Stone, J. D. Joannopoulos, and M. Soljačić. Bound states in the continuum. *Nature Reviews Materials*, 1:1–13, 2016.

[12] L. S. Cederbaum, J. Zobeley, and F. Tarantelli. Gian intermolecular decay and fragmentationof clusters. *Physical Review Letters*, 97(24), 1997.

[13] T. Mitteva, S. Kazandjian, P. Kolorenč, P. Votavová, and N. Sisourat. Interatomic coulombic decay mediated by ultra fast superexchange energy transfer. *Physical Review Letters*, 119(8), 2017.

[14] V. Averbukg, I. B. Müller, and L. S. Cederbaum. Mechanism of interatomic coulomcic decau in clusters. *Physical Review Letters*, 93(26), 2004.

[15] K. Gokhberg, S. Kopelke, N. V. Kryzhevoi, P. Kolorenč, and L. S Cederbaum. Dependence of interatomic decay widths on the symmetry of the decaying state: Analytical expressions and *ab ininito* results. *Physical Review A*, 81(1), 2010.

[16] P. Kolorenč and N. Sisourat. Interatomic coulombic decay widths of helium trimer: *Ab initio* calculations. *The Journal of Chemical Physics*, 143(22), 2015.